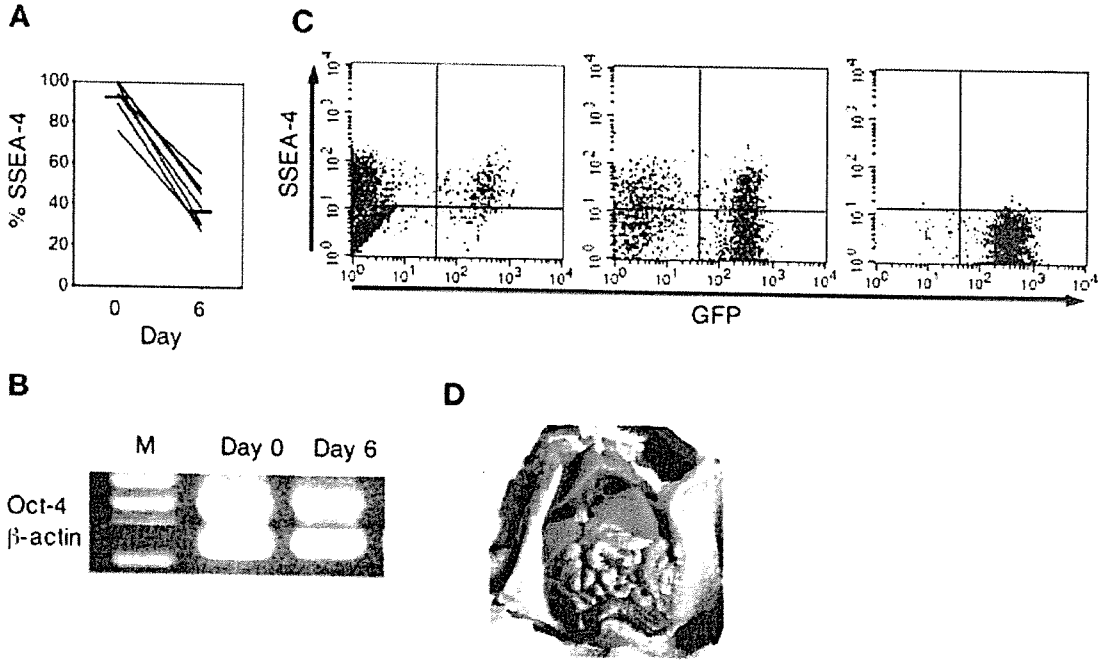

Figure 4. Purging SSEA-4$^+$ cells from among cyESC-derived progenitor cells. **(A):** Undifferentiated cyESCs (day 0) and cyESC-derivatives (day 6) were stained with anti-SSEA-4. The SSEA-4 expression (percentage of total) at day 0 and day 6 is shown (n = 8). **(B):** The Oct-4 expression at days 0 and 6 was also examined by RNA polymerase chain reaction. **(C):** Flow cytometric dot-plot profiles are shown for the SSEA-4 versus GFP expression at day 0 (left), at day 6 before the purge (middle), and at day 6 after the purge (right). Six independent experiments were conducted, and similar results were obtained. **(D):** No tumors were detected in any monkey after the transplantation of SSEA-4-negative day-6 cyESC derivatives (a representative monkey, no. 0981). Abbreviations: cyESC, cynomolgus embryonic stem cell; GFP, green fluorescent protein; M, molecular weight marker; SSEA, stage-specific embryonic antigen.

the fraction was not spoiled (2.3%–5.0%; Table 1), although the removed SSEA-4$^+$ fraction included some CD34$^+$ cells (data not shown).

Discussion

We have previously described a method for hematopoietic engraftment from cyESCs [13]. cyESCs were first cultured for 6 days in vitro, and the day-6 cyESC-derived putative hematopoietic precursors were transplanted in vivo into fetal sheep liver after the first trimester, generating sheep with cynomolgus hematopoiesis. We transplanted the day-6 cells because the CD34 expression level was highest at this time point (Fig. 1C). We transplanted the cells into the liver because the liver is the major hematopoietic organ at this stage of gestation in sheep [34]. In the present study, we tested this method in a cynomolgus monkey allogeneic transplantation model and successfully detected cyESC-derived hematopoietic cells in cynomolgus recipients, albeit at low levels. cyESC-derived chimerism was, however, higher in the primate allogeneic transplantation model (2.3%–5.0%) than in our recently reported sheep xeno-transplantation model (1.1%–1.6%; [13]) (Table 1). To enhance ESC-derived hematopoiesis, further consideration is required of the in vitro culture conditions (i.e., the cytokine milieu, coculture- or embryoid body-associated cellular microenvironment, culture period, and genetic manipulation) and the in utero transplantation conditions (i.e., the preconditioning, route, and timing).

Teratomas developed in all animals, even after the transplantation of ESC-derived progenitor cells that had been cultured for 6 days in the differentiation medium. The risk of tumor formation was high, given that we could hardly detect tumors in immunodeficient mice or fetal sheep that had been transplanted with the same day-6 cyESC derivatives ([13] and our unpublished data). Innate immune responses against cynomolgus-derived tumors might be more rigorous in xeno-transplanted mice and sheep than in allo-transplanted monkeys, resulting in a failure to detect tumorigenesis in the xeno-transplantation models. Similarly, Erdo et al. reported that tumors developed after ESC-derived progenitor cell transplantation in the mouse-to-mouse setting, but not in the mouse-to-rat setting [35]. Our monkey allogeneic transplantation setting would therefore allow the strict evaluation of the in vivo safety of transplantation therapies using ESCs. However, given that teratomas indeed form when undifferentiated cyESCs alone are xeno-transplanted into immunodeficient mice, it is unclear why residual undifferentiated cells included among the day-6 cyESC derivatives did not form teratomas in immunodeficient mice or fetal sheep.

SSEAs that are developmentally regulated during early embryogenesis are widely used as markers to monitor the differentiation of both mouse and human embryos and ESCs [36–38]. Undifferentiated ESCs of both human and cynomolgus origin are characterized by the expression of SSEA-4 and by a lack of SSEA-1 [1, 2, 18]. We have therefore used SSEA-4 as a marker for the negative selection of an undifferentiated fraction. As a result of this negative selection, tumors were no longer detected in the monkeys after transplantation. On the other hand, Bieberich et al. recently developed a method for selective apoptosis of residual pluripotent stem cells using the transcription

factor Oct-4 as a pluripotency marker to prevent teratoma formation [39]. They found that the expression of Oct-4 is colocalized with that of prostate apoptosis response-4, a protein mediating ceramide-induced apoptosis. Treatment of ESC-derived neural precursors with ceramide resulted in selective elimination of residual Oct-4-positive pluripotent cells. Our method, however, uses a cell surface marker to purge pluripotent cells. With this method, one can see the purging efficiency in real-time. This would be meritorious for clinical applications. Although we used a cell sorter to obtain the SSEA-4$^-$ fraction in the present study, selection with beads would be easier and more appropriate for clinical applications.

To generalize the use of SSEA-4 for eliminating undifferentiated cells from among donor cells, we differentiated cyESCs into neural stem cells. After the culture, approximately 10% of cells were still positive for SSEA-4. When all the cells were transplanted into the striatum of Parkinson's cynomolgus monkeys, teratomas developed. We then transplanted cyESC-derived neural stem cells without an SSEA-4$^+$ fraction into the cynomolgus striatum and successfully detected the engraftment without tumor formation (our unpublished data). The removal of SSEA-4$^+$ cells is useful at least for hematopoietic and neural lineages.

CONCLUSION

We are now able to prevent the formation of tumors in nonhuman primate recipients by purging SSEA-4$^+$ cells from among ESC-derived progenitor cells without spoiling the engraftment. SSEA-4 is therefore a clinically relevant pluripotency marker of primate ESCs. Purging pluripotent cells with this marker would be a promising method for producing clinical progenitor cell preparations using hESCs to improve safety in vivo.

ACKNOWLEDGMENTS

We thank Norio Nakatsuji (Kyoto University, Kyoto, Japan) and Yasushi Kondo (Tanabe Seiyaku Co., Ltd., Osaka, Japan) for providing cyESCs; Toru Nakano (Osaka University, Osaka, Japan) for providing OP9 cells; and Naomi Terao and Naomi Takino for technical assistance. This study was supported by grants (JMS 21st Century COE program, High-tech Research Center program, and Creation of Innovations) from the Ministry of Education, Culture, Sports, Science and Technology of Japan as well as grants (KAKENHI) from the Ministry of Health, Labor and Welfare of Japan.

DISCLOSURES

The authors indicate no potential conflicts of interest.

REFERENCES

1 Thomson JA, Itskovitz-Eldor J, Shapiro SS et al. Embryonic stem cell lines derived from human blastocysts. Science 1998;282:1145–1147.

2 Reubinoff BE, Pera MF, Fong CY et al. Embryonic stem cell lines from human blastocysts: Somatic differentiation in vitro. Nat Biotechnol 2000; 18:399–404.

3 Bjorklund LM, Sanchez-Pernaute R, Chung S et al. Embryonic stem cells develop into functional dopaminergic neurons after transplantation in a Parkinson rat model. Proc Natl Acad Sci U S A 2002;99: 2344–2349.

4 Fujikawa T, Oh SH, Pi L et al. Teratoma formation leads to failure of treatment for type I diabetes using embryonic stem cell-derived insulin-producing cells. Am J Pathol 2005;166:1781–1791.

5 Asano T, Ageyama N, Takeuchi K et al. Engraftment and tumor formation after allogeneic in utero transplantation of primate embryonic stem cells. Transplantation 2003;76:1061–1067.

6 Takagi Y, Takahashi J, Saiki H et al. Dopaminergic neurons generated from monkey embryonic stem cells function in a Parkinson primate model. J Clin Invest 2005;115:102–109.

7 Sanchez-Pernaute R, Studer L, Ferrari D et al. Long-term survival of dopamine neurons derived from parthenogenetic primate embryonic stem cells (Cyno-1) after transplantation. STEM CELLS 2005;23: 914–922.

8 Darrasse-Jeze G, Marodon G, Salomon BL et al. Ontogeny of CD4$^+$CD25$^+$ regulatory/suppressor T cells in human fetuses. Blood 2005;105:4715–4721.

9 Harrison MR, Slotnick RN, Crombleholme TM et al. In-utero transplantation of fetal liver haemopoietic stem cells in monkeys. Lancet 1989;2: 1425–1427.

10 Zanjani ED, Mackintosh FR, Harrison MR. Hematopoietic chimerism in sheep and nonhuman primates by in utero transplantation of fetal hematopoietic stem cells. Blood Cells 1991;17:349–366.

11 Cowan MJ, Tarantal AF, Capper J et al. Long-term engraftment following in utero T cell-depleted parental marrow transplantation into fetal rhesus monkeys. Bone Marrow Transplant 1996;17:1157–1165.

12 Tarantal AF, Goldstein O, Barley F et al. Transplantation of human peripheral blood stem cells into fetal rhesus monkeys (*Macaca mulatta*). Transplantation 2000;69:1818–1823.

13 Sasaki K, Nagao Y, Kitano Y et al. Hematopoietic microchimerism in sheep after in utero transplantation of cultured cynomolgus embryonic stem cells. Transplantation 2005;79:32–37.

14 Wang L, Li L, Shojaei F et al. Endothelial and hematopoietic cell fate of human embryonic stem cells originates from primitive endothelium with hemangioblastic properties. Immunity 2004;21:31–41.

15 Flake AW, Harrison MR, Adzick NS et al. Transplantation of fetal hematopoietic stem cells in utero: The creation of hematopoietic chimeras. Science 1986;233:776–778.

16 Takeuchi M, Sekiguchi T, Hara T et al. Cultivation of aorta-gonad-mesonephros-derived hematopoietic stem cells in the fetal liver microenvironment amplifies long-term repopulating activity and enhances engraftment to the bone marrow. Blood 2002;99:1190–1196.

17 Takada T, Suzuki Y, Kondo Y et al. Monkey embryonic stem cell lines expressing green fluorescent protein. Cell Transplant 2002;11:631–635.

18 Suemori H, Tada T, Torii R et al. Establishment of embryonic stem cell lines from cynomolgus monkey blastocysts produced by IVF or ICSI. Dev Dyn 2001;222:273–279.

19 Nakano T, Kodama H, Honjo T. Generation of lymphohematopoietic cells from embryonic stem cells in culture. Science 1994;265:1098–1101.

20 Shibata H, Hanazono Y, Ageyama N et al. Collection and analysis of hematopoietic progenitor cells from cynomolgus macaques (*Macaca fascicularis*): Assessment of cross-reacting monoclonal antibodies. Am J Primatol 2003;61:3–12.

21 Yoshino N, Ami Y, Terao K et al. Upgrading of flow cytometric analysis for absolute counts, cytokines and other antigenic molecules of cynomolgus monkeys (*Macaca fascicularis*) by using anti-human cross-reactive antibodies. Exp Anim 2000;49:97–110.

22 Yoshioka T, Ageyama N, Shibata H et al. Repair of infarcted myocardium mediated by transplanted bone marrow-derived CD34$^+$ stem cells in a nonhuman primate model. STEM CELLS 2005;23:355–364.

23 Zhang WJ, Park C, Arentson E et al. Modulation of hematopoietic and endothelial cell differentiation from mouse embryonic stem cells by different culture conditions. Blood 2005;105:111–114.

24 Vodyanik MA, Bork JA, Thomson JA et al. Human embryonic stem cell-derived CD34$^+$ cells: Efficient production in the coculture with OP9 stromal cells and analysis of lymphohematopoietic potential. Blood 2005;105:617–626.

25 Berenson RJ, Bensinger WI, Hill RS et al. Engraftment after infusion of $CD34^+$ marrow cells in patients with breast cancer or nueroblastoma. Blood 1991;77:1717–1722.

26 Donahue RE, Kirby MR, Metzger ME et al. Peripheral blood $CD34^+$ cells differ from bone marrow $CD34^+$ cells in Thy-1 expression and cell cycle status in nonhuman primates mobilized or not mobilized with granulocyte colony-stimulating factor and/or stem cell factor. Blood 1996;87:1644–1653.

27 Negrin RS, Atkinson K, Leemhuis T et al. Transplantation of highly purified $CD34^+Thy\text{-}1^+$ hematopoietic stem cells in patients with metastatic breast cancer. Biol Blood Marrow Transplant 2000;6:262–271.

28 Nishikawa SI, Nishikawa S, Hirashima M et al. Progressive lineage analysis by cell sorting and culture identifies $FLK1^+VE\text{-}cadherin^+$ cells at a diverging point of endothelial and hemopoietic lineages. Development 1998;125:1747–1757.

29 Schlaeger TM, Mikkola HK, Gekas C et al. Tie2Cre-mediated gene ablation defines the stem cell leukemia gene (SCL/tal1)-dependent window during hematopoietic stem cell development. Blood 2005;105:3871–3874.

30 D'Souza SL, Elefanty AG, Keller G. SCL/Tal-1 is essential for hematopoietic commitment of the hemangioblast but not for its development. Blood 2005;105:3862–3870.

31 Flake AW, Hendrick MH, Rice HE et al. Enhancement of human hematopoiesis by mast cell growth factor in human-sheep chimeras created by the in utero transplantation of human fetal hematopoietic cells. Exp Hematol 1995;23:252–257.

32 Hayashi S, Peranteau WH, Shaaban AF et al. Complete allogeneic hematopoietic chimerisim achieved by a combined strategy of in utero hematopoietic stem cell transplantation and postnatal donor lymphocyte infusion. Blood 2002;100:804–812.

33 Fujiki Y, Fukawa K, Kameyama K et al. Successful multilineage engraftment of human cord blood cells in pigs after in utero transplantation. Transplantation 2003;75:916–922.

34 Miyasaka M, Morris B. The ontogeny of the lymphoid system and immune responsiveness in sheep. Prog Vet Microbiol Immunol 1988;4:21–55.

35 Erdo F, Buhrle C, Blunk J et al. Host-dependent tumorigenesis of embryonic stem cell transplantation in experimental stroke. J Cereb Blood Flow Metab 2003;23:780–785.

36 Shevinsky LH, Knowles BB, Damjanov I et al. Monoclonal antibody to murine embryos defines a stage-specific embryonic antigen expressed on mouse embryos and human teratocarcinoma cells. Cell 1982;30:697–705.

37 Kannagi R, Cochran NA, Ishigami F et al. Stage-specific embryonic antigens (SSEA-3 and -4) are epitopes of a unique globo-series ganglioside isolated from human teratocarcinoma cells. EMBO J 1983;2:2355–2361.

38 Henderson JK, Draper JS, Baillie HS et al. Preimplantation human embryos and embryonic stem cells show comparable expression of stage-specific embryonic antigens. STEM CELLS 2002;20:329–337.

39 Bieberich E, Silva J, Wang G et al. Selective apoptosis of pluripotent mouse and human stem cells by novel ceramide analogues prevents teratoma formation and enriches for neural precursors in ES cell-derived neural transplants. J Cell Biol 2004;167:723–734.

Improved Safety of Hematopoietic Transplantation with Monkey Embryonic Stem Cells in the Allogeneic Setting

Hiroaki Shibata, Naohide Ageyama, Yujiro Tanaka, Yukiko Kishi, Kyoko Sasaki, Shinichiro Nakamura, Shin-ichi Muramatsu, Satoshi Hayashi, Yoshihiro Kitano, Keiji Terao and Yutaka Hanazono

Stem Cells 2006;24;1450-1457; originally published online Feb 2, 2006;
DOI: 10.1634/stemcells.2005-0391

THE JOURNAL OF BIOLOGICAL CHEMISTRY VOL. 280, NO. 38, pp. 32586–32593, September 23, 2005

Interaction of a Small Heat Shock Protein of the Fission Yeast, *Schizosaccharomyces pombe*, with a Denatured Protein at Elevated Temperature*[S]

Received for publication, April 15, 2005, and in revised form, July 25, 2005 Published, JBC Papers in Press, July 29, 2005, DOI 10.1074/jbc.M504121200

Maya Hirose[‡], Hideki Tohda[‡§], Yuko Giga-Hama[§], Reiko Tsushima[‡], Tamotsu Zako[‡], Ryo Iizuka[‡], Changi Pack[¶], Masataka Kinjo[¶], Noriyuki Ishii[‖], and Masafumi Yohda[‡1]

From the [‡]Department of Biotechnology and Life Science, Tokyo University of Agriculture and Technology, 2-24-16, Naka-cho, Koganei-shi, Tokyo 184-8588, [§]ASPEX Division, Asahi Glass Co., Ltd., 1150 Hazawa-cho, Kanagawa-ku, Yokohama-shi, Kanagawa 221-8755, [¶]Laboratory of Supramolecular Biophysics, Research Institute for Electronic Science, Hokkaido University, N12W6, Kita-ku, Sapporo, Hokkaido 060-0812, and the [‖]Biological Information Research Center, National Institute of Advanced Industrial Science and Technology, Tsukuba Central 6, 1-1-1, Higashi, Tsukuba-shi, Ibaraki, 305-8566, Japan

We have expressed, purified, and characterized one small heat shock protein of the fission yeast *Schizosaccharomyces pombe*, SpHsp16.0. SpHsp16.0 was able to protect citrate synthase from thermal aggregation at 45 °C with high efficiency. It existed as a hexadecameric globular oligomer near the physiological growth temperature. At elevated temperatures, the oligomer dissociated into small species, probably dimers. The dissociation was completely reversible, and the original oligomer reformed immediately after the temperature dropped. Large complexes of SpHsp16.0 and denatured citrate synthase were observed by size exclusion chromatography and electron microscopy following incubation at 45 °C and then cooling. However, such large complexes did not elute from the size exclusion column incubated at 45 °C. The denatured citrate synthase protected from aggregation was trapped by a GroEL trap mutant at 45 °C. These results suggest that the complex of SpHsp16.0 and denatured citrate synthase at elevated temperatures is in the transient state and has a hydrophobic nature. Analyses of the interaction between SpHsp16.0 and denatured citrate synthase by fluorescence cross-correlation spectrometry have also shown that the characteristics of SpHsp16.0-denatured citrate synthase complex at the elevated temperature are different from those of the large complex obtained after the shift to lowered temperatures.

Small heat shock protein (sHsps)[2] is one of the ubiquitous chaperones, existing in all types of organisms, including archaea, bacteria, and eukarya (1). sHsps endow thermotolerance to cells *in vivo* (2, 3) and also protect proteins from thermal aggregation and, in some cases, promote the renaturation of proteins *in vitro* (4–6). Compared with other chaperones, they are relatively heterogeneous in sequence and size. They are grouped together based on a conserved domain, the α-crystallin domain, which is named after the α-crystallin of the vertebrate eye lens (7). The α-crystallin domain is preceded by a highly variable N-terminal region and is followed by a short, partly conserved C-terminal extension (8). Although all sHsps exist as large oligomeric complexes, their quaternary structures are diverse and are composed of 9–40 subunits (9). To date, the three-dimensional crystal structures of MjHsp16.5, a sHsp from hyperthermophilic archaeon *Methanococcus jannaschii*, and Hsp16.9, a sHsp from wheat, have been determined. MjHsp16.5 forms a hollow spherical complex of 24 subunits (10), whereas Hsp16.9 exists as a dodecameric double disk (11). The crystal structures show that the α-crystallin domain is composed of β-strands, and the two proteins utilize a similar dimer as a higher assembly building block but differ in their quaternary structure. In contrast, some members of the sHsp family like α-crystallin are remarkably polydisperse (12).

It has been revealed that the molecular mechanism of the chaperone function of sHsps resides in the oligomeric structure. The chaperone potential of sHsps is latent when they exist as large oligomeric structures under physiological conditions. At elevated temperatures, the equilibrium shifts to the dissociated sate, and the hidden hydrophobic substrate-binding sites are exposed to express chaperone activity (13). In the presence of denatured proteins, small oligomers form a large stable complex to protect against aggregation. Recently, Fu *et al.* (14) have shown that a mutant of Hsp16.3 of *Mycobacterium tuberculosis* with nine residues missing from the C terminus that cannot form a large oligomeric complex exhibits chaperone activity at low temperatures. The large substrate-sHsp complexes are dissociated to renature by the action of the DnaK system or more efficiently by the cooperation of DnaK and ClpB system (15–19). In the absence of denatured proteins, dissociated small complexes reassemble into a large oligomer after a shift to physiological temperatures.

In the fission yeast *Schizosaccharomyces pombe*, two small heat shock protein genes (SPCC338.06c and SPBC3E7.02c) have been identified. Expression of SpHsp16.0 (SPBC3E7.02c) is induced by a number of experimental stimuli including heat shock. In addition, its expression is also responsive to depletion of deoxyribonucleotides or DNA damage, and this response is dependent on the *spc1* MAPK pathway and the transcription factor *atf1* (20). SPCC338.06c encodes sHsp with the molecular mass of 15,806 Da, which shares 34.8% amino acid sequence

* This work was supported by the Ministry of Education, Science, Sports, Culture, and Technology through Tokyo University of Agriculture and Technology as part of the 21st Century Center of Excellence program of the "Future Nano-Materials" research and education project. This work was also supported by Grants-in-aid for Scientific Research on Priority Areas 15032212 and 17028013 and by a grant of the National Project on Protein Structural and Functional Analyses from the Ministry of Education, Science, Sports and Culture of Japan (to M. Y.). The costs of publication of this article were defrayed in part by the payment of page charges. This article must therefore be hereby marked "*advertisement*" in accordance with 18 U.S.C. Section 1734 solely to indicate this fact.

[S] The on-line version of this article (available at http://www.jbc.org) contains supplemental Fig. S1.

[1] To whom correspondence should be addressed: Dept. of Biotechnology and Life Science, Tokyo University of Agriculture and Technology, 2-24-16, Naka-cho, Koganei-shi, Tokyo 184-8588, Japan. Tel. and Fax: 81-42-388-7479; E-mail: yohda@cc.tuat.ac.jp.

[2] The abbreviations used are: sHsp, small heat shock protein; CS, citrate synthase; FCS, fluorescence correlation spectroscopy; FCCS, fluorescence cross-correlation spectroscopy; GFP, green fluorescent protein; Cy5-CS, Cy5-labeled CS; SEC-MALS, size exclusion chromatography-multi-angle light scattering; BODIPY, 4,4-difluoro-5,7-dimethyl-4-bora-3a,4a-diaza-s-indacene-3-propionic acid; HPLC, high pressure liquid chromatography.

identity with SpHsp16.0. It is also induced by heat shock.[3] However, their biochemical characterizations have not been performed previously.

In this study, we have expressed and characterized SpHsp16.0. Similar to other sHsps, it existed as a large oligomeric complex and dissociated into small oligomers at elevated temperatures to function as a molecular chaperone. It formed a large complex with a denatured protein after heat incubation like other sHsps. We found that the complex of SpHsp16.0 and denatured protein was in a different state at elevated temperatures. It seems to be in the transient state and have a hydrophobic nature. By fluorescence cross-correlation spectroscopy, the interactions of SpHsp16.0 and a denatured protein at different conditions were compared.

MATERIALS AND METHODS

Proteins, Reagents, and Strains—Ex Taq DNA polymerase, restriction enzymes, and other reagents for gene manipulation were obtained from TAKARA Bio Inc. (Shiga, Japan). Citrate synthase (CS) from porcine heart was purchased from Sigma-Aldrich. GFP was purified as described previously (21). A bacterial chaperonin GroEL trap mutant (D398A-GroEL) ($GroEL_{trap}$) was used to trap an unfolded protein (22). Fluorescent labeling of SpHsp16.0 and CS was performed using BODIPY-FL (4,4-difluoro-5,7-dimethyl-4-bora-3a,4a-diaza-s-indacene-3-propionic acid) succinimidyl ester (Molecular Probes, Eugene, OR) and Cy5 Mono-reactive Dye (Amersham Biosciences). Other reagents were the products of Wako Pure Chemical Industries (Osaka, Japan). *S. pombe* ARC032 (*972h*$^-$) was used for preparation of the genomic DNA. *Escherichia coli* strains DH5α and BL21(DE3) were used for plasmid construction and protein expression, respectively.

Expression and Purification of SpHsp16.0—Because the gene is not split by introns, a full-length gene for SpHsp16.0 was amplified from the total genomic DNA of *S. pombe* ARC032 by PCR using as primers 5′-CCC-ATA-TGT-CTT-TGC-AAC-CTT-TTT-T-3′ and 5′-GGG-AAT-TCT-TAC-TTA-ATA-GCA-ATT-TGT-T-3′ and then subcloned into the pT7Blue T vector. After confirmation of the sequence, the gene was excised with NdeI and EcoRI and then introduced into the NdeI/EcoRI site of pET23b to construct pSpHsp16.0E.

E. coli BL21(DE3) transformed with pSpHsp16.0E was grown at 37 °C in Luria-Bertani medium containing 100 μg/ml of ampicillin. The cells were harvested by centrifugation at 4,600 × *g* for 20 min at 4 °C. The harvested cells were resuspended in buffer A (50 mM Tris-HCl, pH 8.0, 0.1 mM EDTA, and 1 mM dithiothreitol) and disrupted by sonication. Then the suspension of disrupted cells was centrifuged at 25,000 × *g* for 30 min at 4 °C. The supernatant was applied to a DEAE-Toyopearl anion exchange column (Tosoh, Tokyo, Japan) equilibrated with buffer A. The proteins were eluted with a linear gradient of 0–500 mM NaCl in buffer A. Fractions containing SpHsp16.0 were pooled, concentrated by ultrafiltration (Amicon Ultra, Millipore, Billerica, MA), and then applied to a UnoQ6 column (Bio-Rad) equilibrated with buffer A. The proteins were eluted with a linear gradient of 0–500 mM NaCl in buffer A. Fractions containing SpHsp16.0 were pooled, concentrated by ultrafiltration (Amicon Ultra), and then applied to a HiLoad 26/60 Superdex 200-pg size exclusion column (Amersham Biosciences) equilibrated with buffer B (50 mM Tris-HCl, pH 8.0, 1 mM dithiothreitol, and 150 mM NaCl). Fractions containing SpHsp16.0 were collected and then concentrated by ultrafiltration.

Thermal Aggregation Measurements—Thermal aggregation of CS from porcine heart was monitored by measuring light scattering at 500 nm with a spectrofluorometer (FP-6500; Jasco, Tokyo, Japan) at 45 °C. Native CS (150 nM, monomer) was incubated in the assay buffer (50 mM Tris-HCl, pH 8.0) with or without SpHsp16.0. The assay buffer was preincubated at 45 °C and continuously stirred throughout the measurement.

Effect of SpHsp16.0 on Spontaneous Refolding of GFP—GFP was denatured by incubation in acidic buffer (100 mM HCl, 50 mM Tris, 100 mM KCl, and 5 mM dithiothreitol) for 30 min at room temperature. Refolding was started by diluting the denatured GFP to be 50 nM in the dilution buffer (50 mM Tris-HCl, pH 8.0, 100 mM KCl, and 5 mM dithiothreitol) without or with SpHsp16.0 (100 nM or 10 μM). The fluorescence of the refolded GFP was monitored at 510 nm with excitation at 400 nm using a spectrofluorophotometer (FP-6500) with continuous stirring at 45 °C.

Electron Microscopy—An aliquot of SpHsp16.0 or SpHsp16.0-CS complex solution was applied onto specimen grids covered with a thin carbon support film, which had been made hydrophilic by the ion spattering device (HDT-400; JEOL, Tokyo, Japan) and then negatively stained with 1% uranyl acetate for 30 s. The images were recorded by making use of a slow scan CCD camera (Gatan Retractable Multiscan camera) under low electron dose conditions at a magnification of 50,000× in an electron microscope (Tecnai F20; Philips Electron Optics, Hillsboro, OR) operated at 120 kV. The images were analyzed on computers using digital micrography.

Size Exclusion Chromatography-Multi-angle Light Scattering (SEC-MALS)—The purified SpHsp16.0 complex was analyzed by SEC-MALS on a TSKgel $G3000_{XL}$ column (Tosoh) connected with a multi-angle light scattering detector (MINI DAWN; Wyatt Technology, Santa Barbara, CA) and a differential refractive index detector (Shodex RI-101; Showa Denko, Tokyo, Japan) by a HPLC system, PU-980i (JASCO). A 100-μl aliquot of sample was injected into the column and eluted with buffer C (50 mM Tris-HCl, pH 7.0, 150 mM NaCl, and 1 mM dithiothreitol) at 1.0 ml/min. The molecular mass and protein concentration were determined according to the instructional manual (23).

Size Exclusion Chromatography at Elevated Temperatures—Size exclusion chromatography was performed with a column, SB-804HQ (Showa Denko), using a HPLC system, PU-1580i, connected with a multi-wavelength detector MD1515 (JASCO). The purified SpHsp16.0 was diluted to 4 μM in buffer B. A 100-μl aliquot of diluted SpHsp16.0 was heated at the specified temperature for 60 min and then loaded on the column heated at the same temperature. Elution was performed with buffer C at a flow rate of 0.5 ml/min. To examine the reversibility of the dissociation, SpHsp16.0 heated at 45 °C was analyzed by size exclusion chromatography at room temperature after cooling at 4 °C for 30 min.

Labeling SpHsp16.0 and CS with Fluorescent Dyes—Before labeling, both SpHsp16.0 and CS were gel-filtrated on a NAP5 column (Sephadex G-25; Amersham Biosciences) equilibrated with 50 mM sodium phosphate, pH 7.5. Then 200 μl of SpHsp16.0 (3 mg/ml) was mixed with 5 μl of 1 M K_2CO_3 to pH 8.5. Subsequently, BODIPY-FL succinimidyl ester was added to the mixture to 121 μM and incubated for 3 h at room temperature. After the reaction, unreacted BODIPY-FL succinimidyl ester was removed by gel filtration with a NAP5 column. After mixing 200 μl of CS (22.4 μM) with 20 μl of 1 M Na_2HPO_4 to pH 9.0, Cy5 monoreactive dye (Amersham Biosciences) was added to 83 μM, and the mixture was incubated for 3 h at room temperature. Then the unreacted Cy5 monoreactive dye was removed by gel filtration with a NAP5 column. The fluorescent-labeled SpHsp16.0 and CS were designated BODIPY-SpHsp16.0 and Cy5-CS, respectively. BODYPY-SpHsp16.0 exhibited almost same chaperone activity as SpHsp16.0 without modification.

[3] M. Hirose, H. Tohda, Y. Giga-Hama, R. Iizuka, C. Sugino, N. Ishii, and M. Yohda, manuscript in preparation.

Analysis of SpHsp16.0-CS Complex by Size Exclusion Chromatography—The interaction in the native structure was examined by size exclusion chromatography at room temperature. A mixture of 1 μM SpHsp16.0 and 0.2 μM Cy5-CS in buffer B was analyzed with a size exclusion column, SB-804HQ, using a HPLC system PU-1580i with buffer B delivered at the flow rate of 0.5 ml/min. Proteins and Cy5-CS were monitored at the absorbance at 220 and 650 nm, respectively. SpHsp16.0-CS complex was analyzed as follows. SpHsp16.0 solution (1 μM) was heated at 45 °C from 5 min, and the Cy5-CS was added to 0.2 μM. After further incubation at 45 °C, the mixture was analyzed on the column at 45 °C or at room temperature after cooling on ice for 30 min. To examine whether other chaperone can rob denatured CS from SpHsp16.0, $GroEL_{trap}$ was added to the mixture of SpHsp16.0 and Cy5-CS to 1 μM (as tetradecamer) after 30 min of incubation at 45 °C. The mixture was analyzed on the column at 45 °C.

FCS and FCCS Measurement—FCS and FCCS measurements were carried out with a ConfoCor2 (Carl Zeiss, Oberkochen, Germany), which consisted of a CW Ar^+ laser and helium-neon laser, a water immersion objective (C-Apochromat, 40×, 1.2 NA, Carl Zeiss), and two channels of avalanche photodiodes (SPCM-200-PQ; EG&G). BODIPY-FL was excited at 488 nm, and Cy5 was excited at 633 nm. The confocal pinhole diameter was adjusted to 90 μm for 633 nm and 50 μm for 488 nm. The emission signals were split by a dichroic mirror (635-nm beam splitter) and detected at 505–550 nm by the green channel for BODIPY-FL and through a 650-nm-long path filter by the red channel for Cy5.

Measurement was performed using 0.2 μM BODIPY-SpHsp16.0 and 0.05 μM Cy5-CS solutions in 50 mM phosphate buffer, pH 7.5. To measure FCS, 100 μl of each labeled protein solution was used for the measurements separately at room temperature or at 42 °C after 5 min of incubation at 45 °C. FCCS at room temperature was measured using 100 μl of the mixture of both labeled proteins. To examine the interaction at 42 °C, 0.2 μM BODIPY-SpHsp16.0 was incubated at 45 °C for 5 min, and then Cy5-CS was added to 0.05 μM. After a further 5-min incubation at 45 °C, 100 μl of the mixture was subjected to FCCS at 42 °C. The large complex of BODIPY-SpHsp16.0 and Cy5-CS was formed by cooling the mixture at 4 °C for 4 min after 5 min of incubation at 45 °C, and then the FCCS measurement was performed at room temperature.

Data Analysis of FCS and FCCS—The fluorescence autocorrelation functions of the red and green channels, $G_r(\tau)$ and $G_g(\tau)$, and the fluorescence cross-correlation function, $G_c(\tau)$, are calculated using Equation 1,

$$G_x(\tau) = \frac{\langle \delta I_i(t) \cdot \delta I_i(t+\tau) \rangle}{\langle I_i(t) \rangle \langle I_j(t) \rangle} \quad \text{(Eq. 1)}$$

where τ denotes the time delay, I_i is the fluorescence intensity of the red channel ($i = r$) or green channel ($i = g$), and $G_r(\tau)$, $G_g(\tau)$, and $G_c(\tau)$ denote the auto correlation function of red ($i = j = x = r$), green ($i = j = x = g$), and cross-correlation ($i = r$, $j = g$, and $x = c$), respectively. Acquired $G_x(\tau)$ were fitted by a one-, two-, or three-component model as shown in Equation 2,

$$G_x(\tau) = 1 + \frac{1}{N}\sum_i F_i \left(1 + \frac{\tau}{\tau_i}\right)^{-1} \left(1 + \frac{\tau}{s^2\tau_i}\right)^{-1/2} \quad \text{(Eq. 2)}$$

where F_i and τ_i are the fraction and diffusion time of component i, respectively. N is the average number of fluorescent particles in the excitation-detection volume defined by radius w_o and length $2z_o$, and s is the structure parameter representing the ratio $s = z_o/w_o$. The pinhole adjustment of the FCS setup, structural parameter, and detection volume were calibrated for 488- and 633-nm excitation using FCS measurements of rhodamin 6G and Cy5 solution, respectively, with a concentration of 10^{-7} M. Molecular masses of labeled protein could be evaluated with the Stokes-Einstein equation relation for a spherical molecule and with the molecular masses of rhodamin 6G or Cy5 as references (24). The average number of red fluorescent particles (N_r) and green fluorescent particles (N_g), and particles that have both red and green fluorescence (N_c) can be calculated with $N_r = 1/G_r(0)$, $N_g = 1/G_g(0)$, and $N_c = G_c(0)/G_r(0)G_g(0)$, respectively. When N_r and N_g are constant, $G_c(0)$ is directly proportional to N_c. For a quantitative evaluation of the cross-correlation among various samples, $G_c(0)$ is normalized by $G_r(0)$ (cross-ratio; $G_c(0)/G_r(0)$) (25).

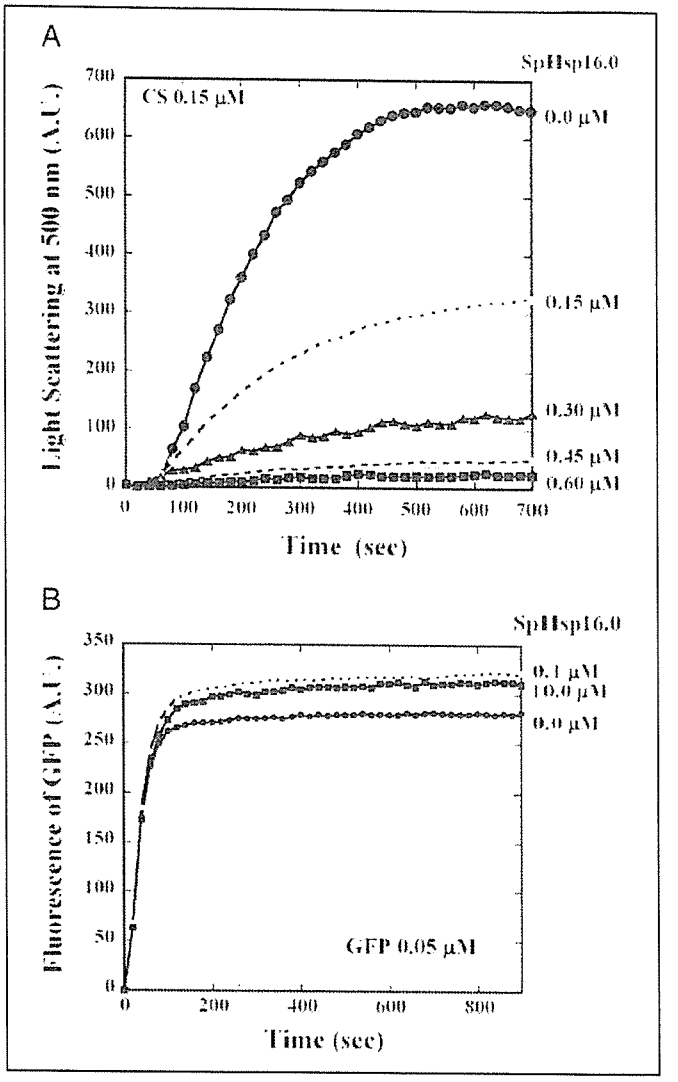

FIGURE 1. **Effects of SpHsp16.0 on thermal aggregation of CS and spontaneous refolding of acid-denatured GFP.** *A*, thermal aggregation of CS from porcine heart was monitored by measuring light scattering at 500 nm using a spectrofluorometer at 45 °C with continuous stirring. Monitoring started with the addition of CS (150 nM as monomer) to 50 mM Tris-HCl buffer, pH 8.0, preincubated at 45 °C without (*closed circle*) or with 150 (*open circle*), 300 (*closed triangle*), 450 (*open triangle*), and 600 nM (*closed square*) SpHsp16.0. *B*, GFP folding was monitored by measuring the fluorescence at 510 nm with excitation at 400 nm using a spectrofluorophotometer. The fluorescence measurement was started by the addition of acid-denatured GFP (final concentration, 50 nM) into the dilution buffer (50 mM Tris-HCl, pH 8.0, 100 mM KCl, 5 mM dithiothreitol) without (*closed circle*) or with 100 nM (*open circle*) or 10 μM (*closed square*) SpHsp16.0 at 45 °C.

RESULTS

SpHsp16.0 Efficiently Protects Porcine Heart Citrate Synthase from Thermal Aggregation but Cannot Arrest Spontaneous Refolding of Acid-

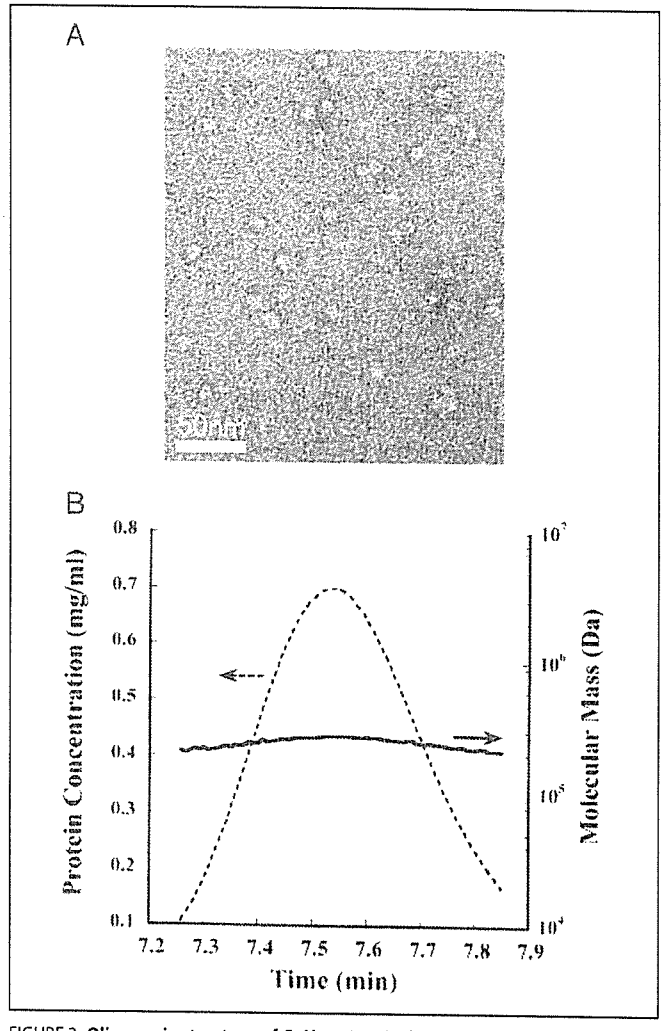

FIGURE 2. **Oligomeric structure of SpHsp16.0.** *A*, electron microscopy of negatively stained SpHsp16.0 is shown. The *bar* represents 50 nm. *B*, the molecular mass of the SpHsp16.0 oligomer was determined by SEC-MALS as described under "Materials and Methods."

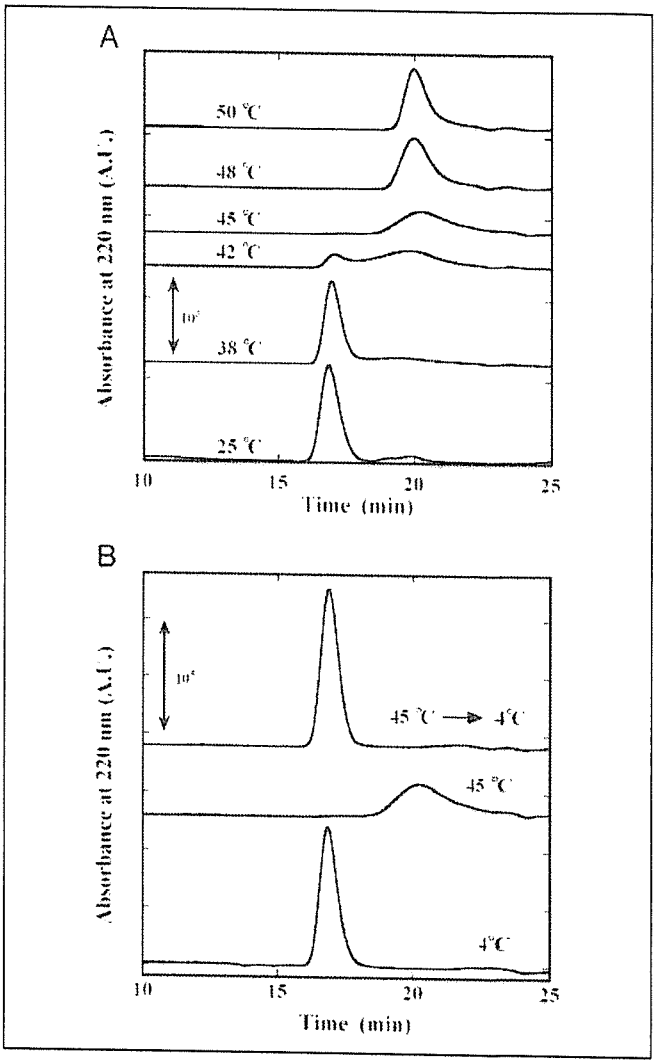

FIGURE 3. **Influence of elevated temperature on SpHsp16.0 oligomeric structure.** Size exclusion chromatography was performed using a SB-804HQ column as described under "Materials and Methods." HPLC analysis of the dissociation of the oligomer at elevated temperatures is shown. *A*, SpHsp16.0 (4 μM) was incubated at the temperature indicated for 60 min and applied to the column, which was kept at the same temperature. *B*, reversibility of the dissociation is shown. To investigate the reversibility of the dissociation, SpHsp16.0 was cooled at 4 °C for 30 min after incubation at 45 °C for 30 min and then applied to the column at room temperature.

denatured GFP—In *S. pombe*, two small heat shock protein genes have been identified. Among them, expression of SPBC3E7.02c is highly induced by a number of experimental stimuli including heat shock. It is named SpHsp16.0 from its deduced molecular mass of 15,967 Da. To examine whether SpHsp16.0 possesses molecular chaperone activity, its effect on the thermal aggregation of CS from porcine heart were examined. As shown in Fig. 1*A*, SpHsp16.0 efficiently prevented the thermal aggregation of CS. An excess of SpHsp16.0 monomer of ~2 mol was enough to suppress the increase in light scattering, which coincides well with previous observations obtained with sHsps from *Saccharomyces cerevisiae* (13, 17). These results support the notion that sHsps function as dimers under heat-stressed conditions.

Then we examined the effects of SpHsp16.0 on the spontaneous refolding of GFP. Chaperonin or prefoldin can capture the folding intermediate of acid denatured GFP and arrest its spontaneous refolding (26, 27). SpHsp16.0 could not suppress the increase of fluorescence even in the presence of a 200-fold excess (Fig. 1*B*). This result suggests that the complex of SpHsp16.0 and denatured protein is not stable as observed for other chaperones.

Oligomeric Structure of SpHsp16.0—Size exclusion chromatography of the purified SpHsp16.0 revealed that it existed as an oligomer. Electron microscopic image of negatively stained SpHsp16.0 showed that it existed as a spherical particle (Fig. 2*A*). The diameter was estimated to be less than 15 nm. The size is almost the same as that of Hsp26 from *S. cerevisiae* (13). Then we determined the molecular mass of the oligomer by SEC-MALS. The molecular mass of the oligomer was calculated to be 250 kDa (Fig. 2*B*). Thus, the SpHsp16.0 oligomer is likely to be composed of 16 subunits.

Temperature-dependent Oligomeric Structural Change of SpHsp16.0—It is postulated that the oligomeric dissociation of sHsp is prerequisite for exposure of the substrate-binding site and then molecular chaperone functions (11, 13, 28–30). We have examined the dissociation of the complex by size exclusion chromatography on HPLC at elevated temperatures. Because we could not observe any structural change when the samples were applied to a column kept at room temperature, analyses were performed with the column heated to the temperature of the sample. As shown in Fig. 3*A*, we observed a temperature-dependent dissociation of the oligomer. At 45 °C, all of the large oligomers disappeared and small complexes appeared.

The dissociation is reversible as shown in Fig. 3*B*. The SpHsp16 oligomer was completely dissociated into small oligomers at 45 °C. The

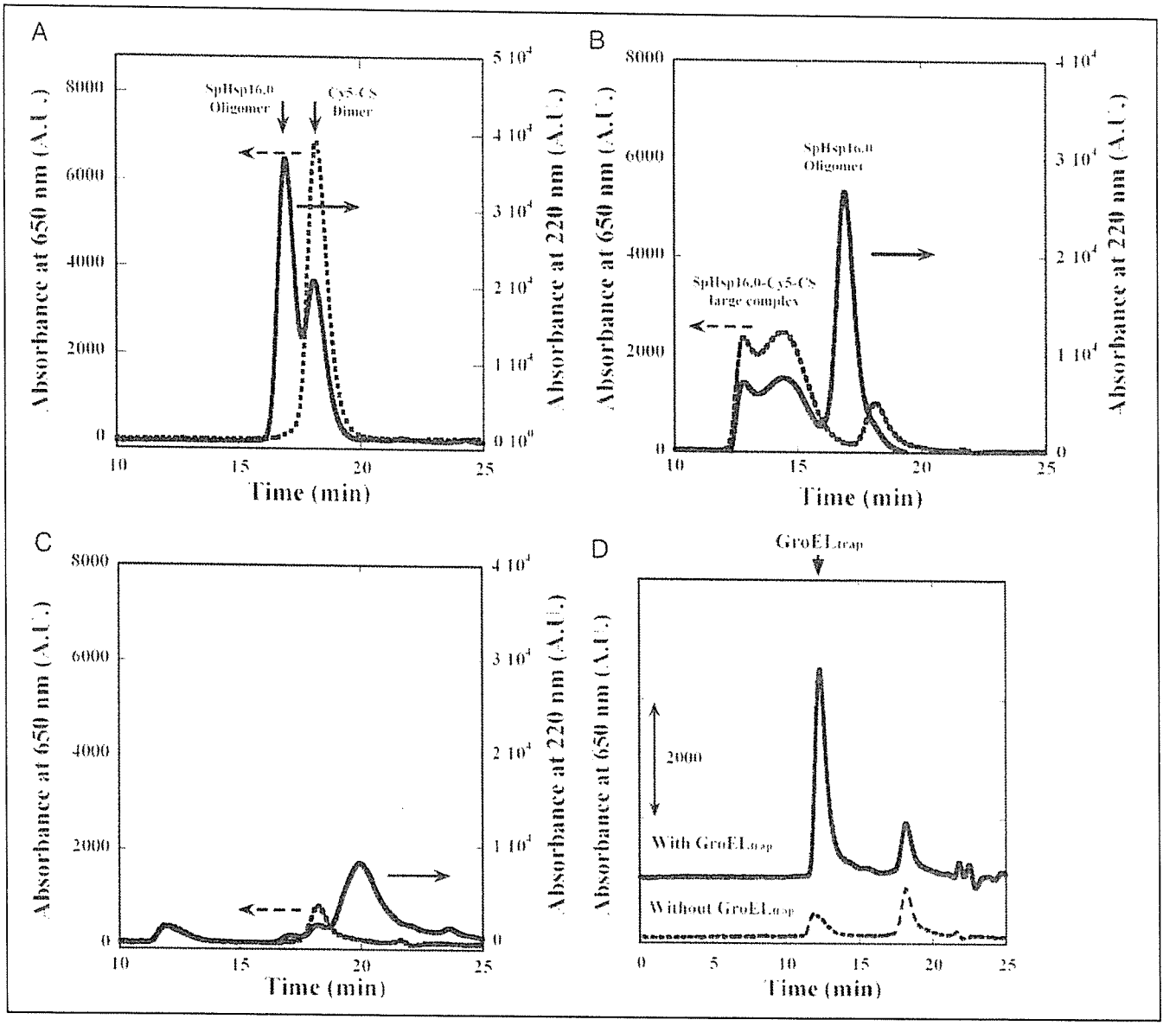

FIGURE 4. **Interaction between SpHsp16.0 and denatured CS.** Interaction of SpHsp16.0 and Cy5-CS was analyzed on a size exclusion column, SB-804HQ, by monitoring the absorbance at 220 and 650 nm. *A*, gel filtration analysis of the mixture of SpHsp16.0 and Cy5-CS at room temperature. *B* and *C*, SpHsp16.0 solution was heated at 45 °C from 5 min, and the Cy5-CS was added. After further incubation at 45 °C, the mixture was analyzed with the column at 45 °C (*C*) or at room temperature after cooling on ice for 30 min (*B*). *D*, GroEL$_{trap}$ was added to the mixture of SpHsp16.0 and Cy5-CS after 30 min incubation at 45 °C, and the mixture was analyzed at 45 °C. As a control, the chromatogram obtained without addition of GroEL$_{trap}$ is also shown. The retention time for GroELtrap is marked.

small oligomers immediately disappeared, and the original oligomeric complex reappeared when the sample was cooled. The dissociation equilibrium is also affected by the concentration as observed for Hsp27 (31) (data not shown). Therefore, we were unable to determine the molecular mass of the small dissociated oligomers by SEC-MALS because of the limit of sensitivity.

Interaction between SpHsp16.0 and Heat-denatured CS—Then interaction between SpHsp16.0 and CS was examined by size exclusion chromatography and electron microscopy. When the mixture of SpHsp16.0 and CS labeled with Cy5 (Cy5-CS) was applied to the size exclusion column without heat treatment, two clearly separated peaks appeared (Fig. 4*A*). The high molecular mass peak corresponds to the SpHsp16.0 oligomer, and the low molecular mass peak corresponds to Cy5-CS (Fig. 4*A*, *dotted line*). Then SpHsp16.0 was incubated with Cy5-CS at 45 °C for 30 min and cooled at 4 °C for 30 min. This mixture was analyzed by size exclusion chromatography at room temperature. Broad and sharp peaks composed of both proteins appeared at shorter elution times (Fig. 4*B*). The large complexes were analyzed by electron microscopy. Various sized elliptical particles of 25–37.5 nm in the major axis, larger than the spherical particles of the SpHsp16.0 oligomer, were observed (Fig. 5). SpHsp16.0 likely binds to non-native CS to form complexes of variable size and shape like other sHsps (13, 17, 29, 32).

Then we examined the complex of SpHsp16.0 and Cy5-CS by the column heated at 45 °C. Unexpectedly, we could not observe any large complexes of SpHsp16.0 and Cy5-CS (Fig. 4*C*). Moreover, most of SpHsp16.0 and Cy5-CS were lost, and only small peaks were observed. The proteins were eluted from the column afterward by washing with ethylene glycol, which is thought to weaken hydrophobic interaction (data not shown). The result suggests that the complex of SpHsp16.0 and Cy5-CS is in the transient state and has hydrophobic nature at elevated temperatures. The observed stable large complex of SpHsp16.0 and CS is likely to be formed after the shift to the nonstress temperature.

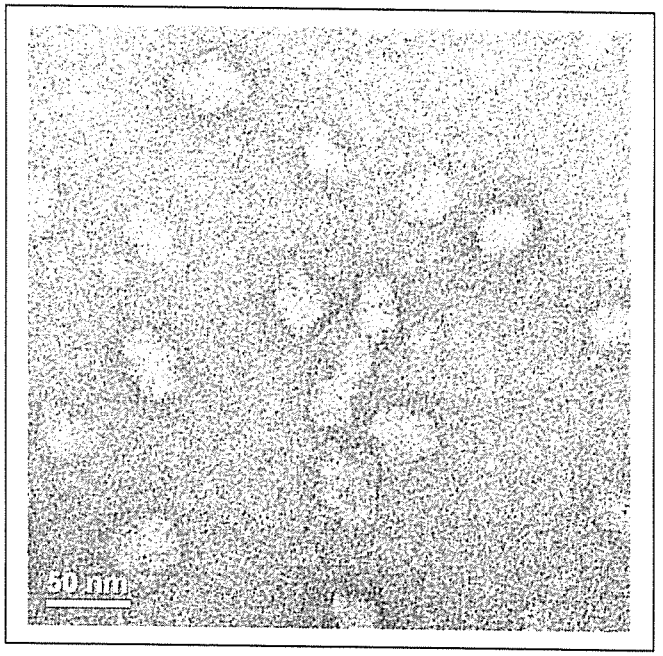

FIGURE 5. **Electron microscopy of the complex of SpHsp16.0 and denatured CS.** The size exclusion chromatography fraction corresponds to the large complex of SpHsp16.0 and CS obtained in the same procedure as for Fig. 6*C* was used for electron microscopy. The *bar* represents 50 nm.

To examine the state of the complex at the elevated temperatures, we examined whether GroEL trap mutant ($GroEL_{trap}$, D398A-GroEL) can rob the denatured Cy5-CS from SpHsp16.0. $GroEL_{trap}$ can capture an unfolded protein but is unable to renature it in an ATP-dependent manner (22). As shown in Fig. 4*D*, most of the fluorescence intensity of Cy5-CS was observed at the position where $GroEL_{trap}$ appeared, indicating that the complex of SpHsp16.0 and denatured Cy5-CS is not stable in the elevated temperature, and binding of denatured protein is likely to be in the dynamic equilibrium state.

Detection of Interaction between SpHsp16.0 and CS at Elevated Temperature by FCS and FCCS—We did not observe a complex of SpHsp16.0 and CS at elevated temperatures by size exclusion chromatography or other methods probably because the complex is in the transient state and also because of the highly hydrophobic nature of the complex. FCS is used to analyze the interaction of proteins in solution (33, 34). It provides information about the diffusion properties of fluorescently tagged target molecules at a very low concentration (pM). FCS measurements are based on single photon counting of fluorescence in a defined detection volume (~0.25 fl) generated by a laser beam and fine detection optics. The diffusion constant and the concentration of target molecule can be determined from the autocorrelation function ($G(\tau)$), allowing us to monitor the interaction *in situ*.

Fig. 6 (*A* and *B*) shows the results of FCS analyses of BODIPY-SpHsp16.0 and Cy5-CS at room temperature and 42 °C. Molecular masses were estimated from the calculated diffusion time using the Einstein-Stokes equation with rhodamin 6G or Cy5 as a standard. At room temperature, the diffusion times of rhodamin 6G, Cy5, BODIPY-SpHsp16.0, and Cy5-CS were 26, 42, 241, and 224 μs, respectively. So the molecular masses of BODIPY-SpHsp16.0 and Cy5-CS were calculated to be 384 and 119 kDa, respectively. Although these values do not exactly match the molecular masses of the SpHsp16.0 hexadecamer (250 kDa) and CS dimer (98 kDa) determined by SEC-MALS or calculated from the amino acid sequences, they reflect well the quaternary structures. When the temperature was increased to 42 °C, both proteins exhibited a dramatic change in diffusion time. The diffusion time of

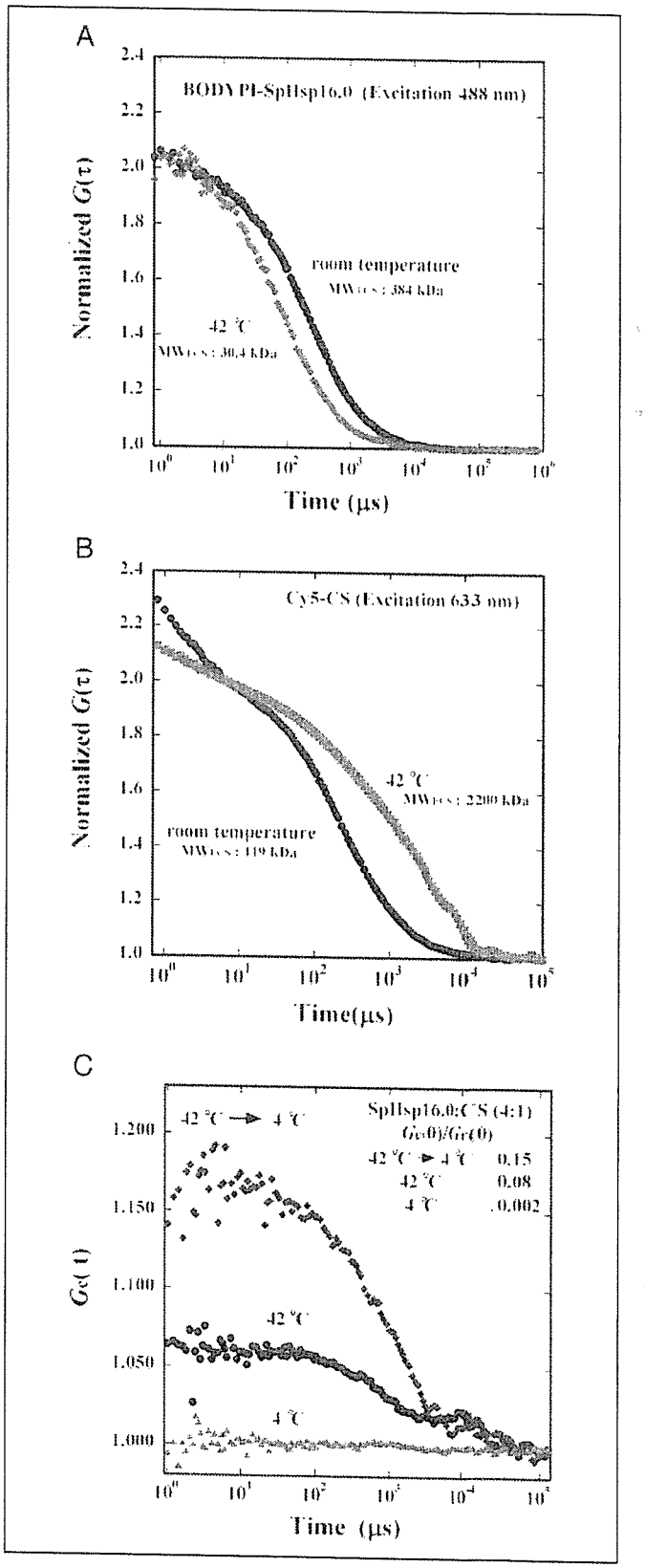

FIGURE 6. **FCS analysis of labeled protein and cross-correlation analysis of molecular interactions.** *A* and *B*, comparison with normalized autocorrelation functions of BODYPY-SpHsp16.0 (*A*) and Cy5-CS (*B*) at room temperature (*closed circle*) and 42 °C (*closed square*). Molecular masses (MW_{FCS}) calculated from diffusion times at room temperature and 42 °C are shown. *C*, cross-correlation functions between BODYPY-SpHsp16.0 and Cy5-CS at 4 °C (*closed triangle*), at 42 °C (*closed circle*), and at 4 °C after heat treatment (*closed square*). Relative cross-correlation amplitudes $G_c(0)/G_r(0)$ are shown.

BODIPY-SpHsp16.0 was 103 μs (corrected for room temperature). Cy5-CS was composed of three components whose diffusion times were 589, 137, and 80 μs. Their distribution ratios were estimated to be 70, 20, and 10%, respectively. The estimated molecular mass of BODIPY-SpHsp16.0 decreased to 30.4 kDa, almost the same as the molecular mass of the dimer, 32 kDa. In contrast, the quaternary structure of CS was not uniform. The molecular mass of the main component is calculated to be ~2200 kDa, which is consistent with the formation of an aggregate.

An extended technique of FCS, FCCS, can detect the coincidence of two spectrally distinct fluorescent probes in a small detection area at very low concentrations. FCCS has been used to detect the association-dissociation reaction and interaction between two molecular species. When 100 μl of a mixture containing BODIPY-SpHsp16 (0.2 μM as monomer) and Cy5-CS (0.05 μM as monomer) was observed at room temperature, almost no cross-correlation between them was observed at room temperature ($G_c(0)/G_r(0) = 0.002$) (Fig. 6*C*). No specific cross-correlation between BODIPY-SpHsp16.0 and only Cy5 dye was observed at room temperature, at 45 °C with cooling to 4 °C, and at 42 °C, respectively (data not shown). By contrast, a significant cross-correlation ($G_c(0)/G_r(0) = 0.15$) was observed when they were incubated at 45 °C and cooled to 4 °C (Fig. 4*C*). The result coincides with the formation of a large complex. Then we performed FCCS at 42 °C, the upper temperature limit of the thermostatted stage of the system. Although the efficiency was relatively low, SpHsp16.0 could suppress the thermal aggregation of CS at that temperature (data not shown). As shown in Fig. 6*C*, a cross-correlation between them was clearly detected ($G_c(0)/G_r(0) = 0.08$). The interaction was not as tight as that observed for the large oligomeric complexes obtained after the temperature shift. Thus, we concluded that the complex of SpHsp16.0 and denatured CS should be different from that observed after the temperature drop.

DISCUSSION

SpHsp16.0 shares almost the same characteristics as other sHsps studied so far. It exists as a large oligomeric complex and dissociated into small oligomers at elevated temperatures. The dissociation is completely reversible in the absence of denatured protein. At the medium temperatures, SpHsp16.0 eluted as broad peaks between the original complex and dissociated species, suggesting that SpHsp16.0 was in the equilibrium between complex and dissociation states. The dissociation equilibrium was also affected by the concentration. We could not determine the molecular mass of the dissociated species by SEC-MALS because they were observed only the concentration is low. Molecular mass estimated from the diffusion constant observed by FCS suggests that the small species is dimer. However, further study would be required to determine the structure of sHsp in the dissociated state.

SpHsp16.0 forms a large complex with CS after the heat incubation and cooling. The complex was stable and did not dissociate spontaneously (data not shown). We could not observe such large complexes of SpHsp16.0 and denatured CS by size exclusion chromatography at 45 °C in spite of the fact that the stable large complex was separated by the column. The result seems to contradict with the previous result of Hsp26 that large complexes with denatured proteins were observed by native PAGE at the high temperature (13). The difference is likely to be caused by the hydrophobic nature of the complex at the high temperature. In our experiment, large portions of SpHsp16.0 and CS were lost during size exclusion chromatography, probably by the hydrophobic interaction. Stable large complexes obtained after the temperature drop did not exhibit such hydrophobic nature, and they eluted quantitatively in size exclusion chromatography.

The difference in the characteristics of the complexes before and after cooling was also observed by FCCS. Compared with the stable complex, the interaction between SpHsp16.0 and Cy5-CS of the complex at the elevated temperature is relatively weak. The hydrophobic nature and the relatively weak interaction suggest that the complex is in the transient state. Binding between SpHsp16.0 and denatured proteins should be in the dynamic equilibrium, resulting in that the surface of the complex is hydrophobic. It is also confirmed by the fact that denatured CS that is protected from aggregation is captured by $GroEL_{trap}$. Incompetence of capturing folding intermediate of GFP is also likely to be due to the same reason because acid denatured GFP folds relatively rapidly compared with *de novo* folding.

We monitored the decrease of CS activity at 45 °C in the absence or presence of 4-fold molar excess SpHsp16.0 (data not shown). CS activity decreased with the incubation time and was almost completely lost after 5 min of incubation. Similar to the result obtained with Hsp25 (17), the presence of SpHSp16.0 had almost no effect on thermal inactivation of CS, even though it can prevent their thermal aggregation. Thus, we think that SpHsp16.0 binds with CS in the irreversibly unfolded state.

Recently, Franzmann *et al.* (35) reported that dissociation of the oligomer is not required for activation of Hsp26. They propose existence of two alternative conformations for the Hsp26 oligomer with different affinities for unfolded proteins. Even though we could not observe such conformational changes of SpHsp16.0 oligomers at elevated temperatures, the existence of SpHsp16.0-substrate complex in the transient state with high affinity implies the presence of the conformation with high affinity.

To reveal the molecular mechanism of chaperone activity of small heat shock proteins, structural and functional characterization of the complex in the transient state would be necessary. Because it is difficult to characterize the transient complex by conventional methods because of high hydrophobicity, we believe that FCS and FCCS are important tools for further study.

REFERENCES

1. Narberhaus, F. (2002) *Microbiol. Mol. Biol. Rev.* **66,** 64–93
2. van den, I. P. R., Overkamp, P., Knauf, U., Gaestel, M., and de Jong, W. W. (1994) *FEBS Lett.* **355,** 54–56
3. Plesofsky-Vig, N., and Brambl, R. (1995) *Proc. Natl. Acad. Sci. U. S. A.* **92,** 5032–5036
4. Horwitz, J. (1992) *Proc. Natl. Acad. Sci. U. S. A.* **89,** 10449–10453
5. Jakob, U., Gaestel, M., Engel, K., and Buchner, J. (1993) *J. Biol. Chem.* **268,** 1517–1520
6. Muchowski, P. J., and Clark, J. I. (1998) *Proc. Natl. Acad. Sci. U. S. A.* **95,** 1004–1009
7. Caspers, G. J., Leunissen, J. A., and de Jong, W. W. (1995) *J. Mol. Evol.* **40,** 238–248
8. Leroux, M. R., Ma, B. J., Batelier, G., Melki, R., and Candido, E. P. (1997) *J. Biol. Chem.* **272,** 12847–12853
9. Buchner, J., Ehrnsperger, M., Gaestel, M., and Walke, S. (1998) *Methods Enzymol.* **290,** 339–349
10. Kim, K. K., Kim, R., and Kim, S. H. (1998) *Nature* **394,** 595–599
11. van Montfort, R. L., Basha, E., Friedrich, K. L., Slingsby, C., and Vierling, E. (2001) *Nat. Struct. Biol.* **8,** 1025–1030
12. Haley, D. A., Bova, M. P., Huang, Q. L., McHaourab, H. S., and Stewart, P. L. (2000) *J. Mol. Biol.* **298,** 261–272
13. Haslbeck, M., Walke, S., Stromer, T., Ehrnsperger, M., White, H. E., Chen, S., Saibil, H. R., and Buchner, J. (1999) *EMBO J.* **18,** 6744–6751
14. Fu, X., Zhang, H., Zhang, X., Cao, Y., Jiao, W., Liu, C., Song, Y., Abulimiti, A., and Chang, Z. (2005) *J. Biol. Chem.* **280,** 6337–6348
15. Lee, G. J., and Vierling, E. (2000) *Plant Physiol.* **122,** 189–198
16. Mogk, A., Deuerling, E., Vorderwulbecke, S., Vierling, E., and Bukau, B. (2003) *Mol. Microbiol.* **50,** 585–595
17. Ehrnsperger, M., Graber, S., Gaestel, M., and Buchner, J. (1997) *EMBO J.* **16,** 221–229
18. Veinger, L., Diamant, S., Buchner, J., and Goloubinoff, P. (1998) *J. Biol. Chem.* **273,** 11032–11037
19. Mogk, A., Schlieker, C., Friedrich, K. L., Schonfeld, H. J., Vierling, E., and Bukau, B. (2003) *J. Biol. Chem.* **278,** 31033–31042
20. Taricani, L., Feilotter, H. E., Weaver, C., and Young, P. G. (2001) *Nucleic Acids Res.* **29,** 3030–3040
21. Iizuka, R., Yoshida, T., Maruyama, T., Shomura, Y., Miki, K., and Yohda, M. (2001) *Biochem. Biophys. Res. Commun.* **289,** 1118–1124
22. Rye, H. S., Burston, S. G., Fenton, W. A., Beechem, J. M., Xu, Z., Sigler, P. B., and Horwich, A. L. (1997) *Nature* **388,** 792–798

23. Wyatt, P. J. (1993) *Anal. Chim. Acta* **272,** 1–40
24. Pack, C. G., Nishimura, G., Tamura, M., Aoki, K., Taguchi, H., Yoshida, M., and Kinjo, M. (1999) *Cytometry* **36,** 247–253
25. Saito, K., Wada, I., Tamura, M., and Kinjo, M. (2004) *Biochem. Biophys. Res. Commun.* **324,** 849–854
26. Okochi, M., Yoshida, T., Maruyama, T., Kawarabayasi, Y., Kikuchi, H., and Yohda, M. (2002) *Biochem. Biophys. Res. Commun.* **291,** 769–774
27. Yoshida, T., Kawaguchi, R., Taguchi, H., Yoshida, M., Yasunaga, T., Wakabayashi, T., Yohda, M., and Maruyama, T. (2002) *J. Mol. Biol.* **315,** 73–85
28. Gu, L., Abulimiti, A., Li, W., and Chang, Z. (2002) *J. Mol. Biol.* **319,** 517–526
29. Usui, K., Ishii, N., Kawarabayasi, Y., and Yohda, M. (2004) *Protein Sci.* **13,** 134–144
30. Fu, X., and Chang, Z. (2004) *Biochem. Biophys. Res. Commun.* **316,** 291–299
31. Shashidharamurthy, R., Koteiche, H. A., Dong, J., and McHaourab, H. S. (2005) *J. Biol. Chem.* **280,** 5281–5289
32. Lee, G. J., Roseman, A. M., Saibil, H. R., and Vierling, E. (1997) *EMBO J.* **16,** 659–671
33. Rigler, R., Mets, U., Widengern, P., and Kask, P. (1993) *Eur. Biophys. J.* **22,** 169–175
34. Pack, C. G., Aoki, K., Taguchi, H., Yoshida, M., Kinjo, M., and Tamura, M. (2000) *Biochem. Biophys. Res. Commun.* **267,** 300–304
35. Franzmann, T. M., Wühr, K., Richter, K., Walter, S., and Buchner, J. (2005) *J. Mol. Biol.* **350,** 1083–1093

厚生労働科学研究研究費補助金

こころの健康科学研究事業

アミロスフェロイド仮説によるアルツハイマー病病態解明と臨床応用に関する研究
-高等動物モデル構築と生体リアルタイム観測法開発によるアプローチ

平成１６～１８年度　総合研究報告書

主任研究者　星　美奈子

平成１９（２００７）年　４月

2/2 冊

Amphiphilic *p*-sulfonatocalix[4]arene-coated CdSe/ZnS quantum dots for the optical detection of the neurotransmitter acetylcholine†

Takashi Jin,*[a] Fumihiko Fujii,[b] Hiroshi Sakata,[b] Mamoru Tamura[a] and Masataka Kinjo[a]

Received (in Cambridge, UK) 12th May 2005, Accepted 3rd June 2005
First published as an Advance Article on the web 11th July 2005
DOI: 10.1039/b506608e

Water-soluble CdSe/ZnS (core–shell) semiconductor quantum dots surface-modified with tetrahexyl ether derivatives of *p*-sulfonatocalix[4]arene were synthesized for the optical detection of the neurotransmitter acetylcholine.

Colloidal quantum dots (QDs) have recently attracted considerable attention as a new class of fluorophores for chemical and biological applications.[1] QDs are semiconductor nanoparticles that have all three dimensions confined to the 2–15 nm length scale.[2] The optical properties of QDs have significant advantages compared with traditional organic fluorescent dyes. QDs are highly bright fluorophores, and they are highly resistant to photobreaching, making them useful for continuous monitoring of fluorescence intensity.[1,2] Besides, QDs have size-tunable narrow emission spectra (typical full width at half maximum <30 nm) in addition to broad excitation spectra.[3] This unique optical property allows a single-light source excitation for multi-colour emission of QDs. Since the first reports[4] of the use of QDs as fluorescent bioprobes in 1998, many applications of QDs have been reported in the field of cellular and biomedical imaging.[3,5]

In contrast, less attention has been paid to the use of QDs as fluorescent probes for chemical and biochemical sensing. So far, several reports of QD-based ion probes have appeared for the fluorescence sensing of metal ions, such as Ag^+, Cu^{2+}, Cd^{2+}, Co^{2+}, and Zn^{2+}.[6] A recent paper has shown the highly sensitive determination of cyanide ions by using CdSe QDs in aqueous solutions.[7] However, possible applications of the QD-based fluorescent probes of biologically important ions or molecules are virtually unexplored. It is well known that the fluorescence efficiency of QDs is sensitive to the presence and nature of adsorbates at the surface of QDs.[1a] Therefore, it is expected that a chemical sensing system based on QDs can be developed using fluorescence changes induced by molecular recognition at the surface of QDs.

Here, we report an optical detection system for the neurotransmitter acetylcholine (ACh) using water-soluble CdSe/ZnS quantum dots surface-modified with tetrahexyl ether derivatives of *p*-sulfonatocalix[4]arene **3** (Scheme 1).

CdSe/ZnS QDs were prepared in a two-step process (ESI†). First, CdSe QDs were synthesized using a method reported by Qu and Peng[8] with a high temperature reaction in a trioctylphosphine oxide (TOPO)–hexadecylamine mixture. Then, the CdSe core was overcoated with a ZnS shell using TOPO as a solvent according to previously published methods.[9] The resulting CdSe/ZnS QDs were capped with TOPO molecules, and they were highly hydrophobic and insoluble in aqueous media.

To prepare water-soluble CdSe/ZnS QDs, we used amphiphilic *p*-sulfonatocalix[4]arenes **1–3** (Scheme 1) as surface-coating agents for the TOPO capped QDs. *p*-Sulfonato[4]calixarene **1** is known to have the ability to bind the quaternary ammonium cation moiety of ACh by its hydrophobic cavity of the aromatic rings.[10] On the basis of this finding, we expected that if TOPO capped QDs could be coated by amphiphilic *p*-sulfonatocalix[4]arenes to form water-soluble QDs, the resulting QDs would have complexing abilities towards ACh at the surface of the QDs.

p-Sulfonatocalix[4]arenes **1** was purchased from Tokyo Kasei Chemicals (Japan) and its derivatives, **2** and **3** were prepared according to the literature method (ESI†).[11] The surface-coating of TOPO capped CdSe/ZnS QDs was performed by mixing the hydrophobic QDs and **1–3** in tetrahydrofuran at room temperature (ESI†). When **1** and **2** were used as the surface-coating agents, the resulting QDs showed very week emission, and they precipitated after several hours in water. In the case of **3**, highly fluorescent and stable, water-soluble QDs were obtained.

Fig. 1 shows the fluorescence spectrum of **3**-coated CdSe/ZnS QDs in water. For comparison, the fluorescence spectrum of water-soluble CdSe/ZnS QDs coated by mercaptoacetic acid (MAA) is also shown. MAA is one of the widely used surface-coating agents used to prepare water-soluble monodisperse QDs.[1] The emission efficiency of the **3**-coated QDs is higher than that of the MAA-coated QDs by a factor of about 3. The quantum yield was estimated as 0.1 using Rhodamine 6G as standard. The spectral width (28 nm) of the **3**-coated QDs is almost the same as that of MAA-coated QDs, indicating that the **3**-coated QDs are monodisperse particles similar to the case of MAA-coated QDs.

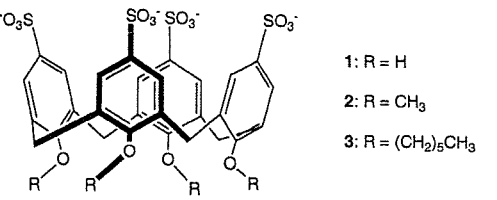

Scheme 1 *p*-Sulfonatocalix[4]arene (**1**) and its derivatives (**2**, **3**).

[a]*Section of Intelligent Materials and Devices, Research Institute for Electronic Science, Hokkaido University, Sapporo, 060-0812, Japan. E-mail: jin@imd.es.hokudai.ac.jp; Fax: +81-11-706-4964; Tel: +81-11-706-2886*
[b]*Innovation Plaza Hokkaido, Japan Science and Technology Agency, Sapporo, 060-0819, Japan. Fax: +81-11-708-1614; Tel: +81-11-708-1614*
† Electronic supplementary information (ESI) available: experimental details for the preparation of QDs and tetrahexyl ether derivatives of *p*-sulfonatocalix[4]arene **3**, ^{1}H NMR data for **3**, and the surface-coating method using **3**. See http://dx.doi.org/10.1039/b506608e

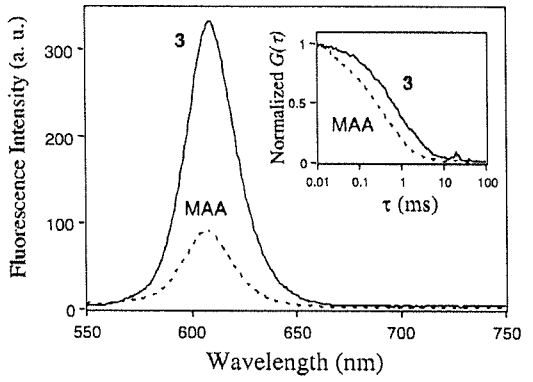

Fig. 1 Fluorescence emission spectra of **3**- and MAA-coated CdSe/ZnS QDs in water. Inset shows fluorescence correlation curves for the QDs in tetraborate buffer (pH = 9.2). The absorbance at 480 nm (excitation wavelength) was adjusted to be 0.05.

To estimate the hydrodynamic size of the QDs, fluorescence correlation spectroscopy (FCS)[12] was used. FCS measures the fluctuation of the fluorescence intensity of fluorophores at the single molecule level in solution. From the analysis of the fluorescence autocorrelation function $G(\tau)$,[13] the diffusion times of the fluorophores can be determined. The $G(\tau)$ curves were measured by using a compact FCS system (C9413, Hamamatsu Photonics, Japan).

The inset in Fig. 1 shows the normalized $G(\tau)$ curves for **3**- and MAA-coated QDs in aqueous solution. The $G(\tau)$ curves were analyzed using a simple one-component diffusion model.[14] The diffusion time of the **3**- and MAA-coated QDs was found to be 0.65 and 0.25 ms, respectively. By using the value of the diffusion time (0.74 ms) measured for 14 nm fluorescent latex beads (Molecular Probes, Inc. USA), the hydrodynamic sizes were calculated to be 12 and 4.7 nm in diameter for **3**- and MAA-coated QDs, respectively.[15]

In the cases of the surface-coating with thiol compounds, it has been shown that the TOPO molecules passivating the QD surface are exchanged with the thiol compounds[1b,c] (Fig. 2). Assuming the molecular length of MAA as 0.35 nm,[16] the size of the semiconductor core of the MAA-coated CdSe/ZnS QDs is estimated as at least 4.0 nm in a diameter. Thus, in the **3**-coated CdSe/ZnS QDs, the length of the surface-coating layer should be 3.6–4 nm, suggesting that the amphiphilic *p*-sulfonatocalix[4]arene molecules form a bilayer structure[17,18] with the TOPO molecules surrounding the QDs (Fig. 2). The higher emission efficiency observed for **3**-coated QDs in comparison with MAA-coated QDs may be explained by a higher barrier towards the access of water molecules to the QD surface. In fact, it has been shown that a surface coating of thiol compounds with longer alkyl chains results in water-soluble CdSe/ZnS QDs with higher emission efficiencies.[18]

In the **3**-coated CdSe/ZnS QDs, the QD surface is covered with the negative charges of the sulfonyl groups. Thus, we first examined the effect of metal cations such as Na^+ and K^+ on the fluorescence spectrum of **3**-coated QDs. The addition of these cations to the colloidal solution (1 mg/20 mL) of **3**-coated QDs did not cause any changes in the fluorescence spectrum, even at a high concentration of 100 mM. Ammonium cations (100 mM) also did not affect the fluorescence spectrum of the QDs. The addition of ACh caused significant changes in the fluorescence spectrum of **3**-coated QDs. Fig. 3 shows the effect of increasing concentrations of ACh on the fluorescence spectrum of the QDs, where its absorbance at 480 nm (excitation wavelength) is adjusted to be 0.05. As can be seen, the fluorescence of the QDs is strongly quenched by ACh. In the presence of 1×10^{-3} M of ACh, fluorescence quenching of *ca.* 50% was observed. It should be noted that the addition of ACh does not change the spectral widths and the emission maximum of the QDs. This finding indicates that ACh does not cause surface deterioration or aggregation in the **3**-coated QDs.

To get insight of the quenching mechanism by ACh, the temperature dependence of the fluorescence quenching was examined (inset in Fig. 3). The results show upward-curving Stern–Volmer plots at 25 and 50 °C, indicating the quenching process contains both a static and dynamic mechanism.[19] It is observed that the quenching efficiency at 50 °C is much larger than that of the lower temperature of 25 °C. This temperature dependence suggests that the quenching is mainly caused by a dynamic mechanism: ACh molecules bound in **3** at the water–QD interface diffuse into the organic layer of the coating, and they may

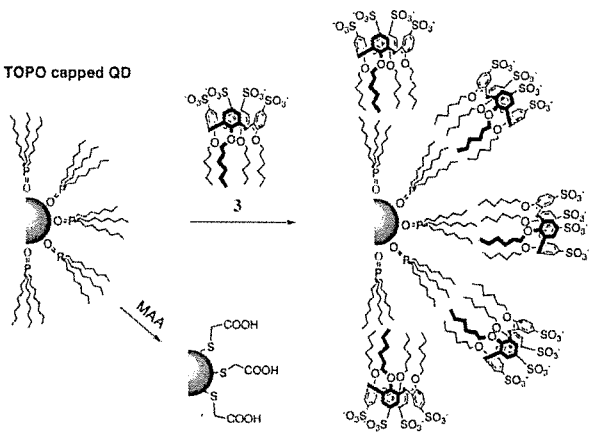

Fig. 2 A schematic representation of the surface-coating of TOPO capped CdSe/ZnS QDs with **3** and MAA.

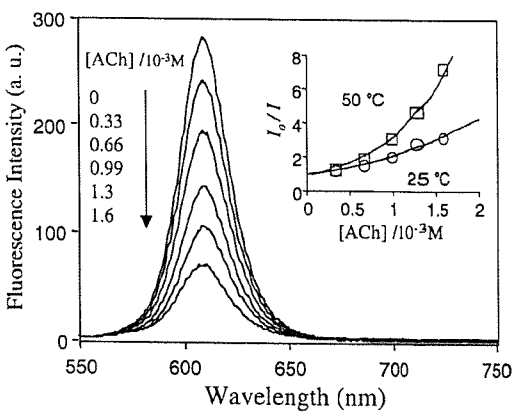

Fig. 3 Quenching of the fluorescence emission of **3**-coated CdSe/ZnS QDs by addition of ACh. Inset shows the Stern–Volmer plots at 25 and 50 °C.

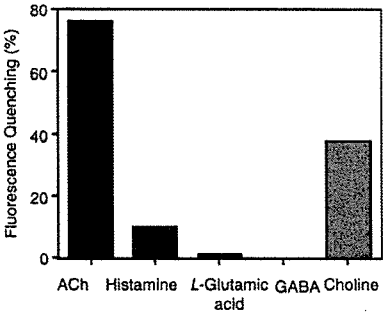

Fig. 4 Fluorescence quenching (I/I_0) of **3**-coated CdSe/ZnS QDs (PBS solution, pH = 7.4) in the presence of neurotransmitter compounds and choline (1.6 mM).

interact with the semiconductor surface to reduce the core electron–hole recombination.

Fluorescence quenching of **3**-coated CdSe/ZnS QDs was examined for several neurotransmitter compounds and choline that is the hydrolyzed product of ACh (Fig. 4). The fluorescence quenching of the **3**-coated QDs is quite selective to ACh among the neurotransmitter compounds tested. The anionic and neutral neurotransmitters (L-glutamic acid and GABA) do not affect the fluorescence spectra of **3**-coated QDs. These neurotransmitters may not have access to the QD surface due to the anionic charges of the sulfonyl groups of **3**. In contrast, the monoamine neurotransmitter histamine with a cationic charge causes a fluorescence quenching of *ca.* 10%, and choline causes a fluorescence quenching of *ca.* 40%. The fact that choline acts as an effective quencher indicates that **3** recognizes the quaternary ammonium cation moiety of choline as well as ACh. The higher quenching efficiency of ACh in comparison with choline can be attributed to its higher hydrophobicity which increases the affinity of ACh towards **3**.[10c]

In summary, we have presented water-soluble CdSe/ZnS QDs surface-modified with amphiphilic *p*-sulfonatocalix[4]arene **3** for the optical detection of the neurotransmitter ACh. To the best of our knowledge, this is the first use of QDs for the detection of neurotransmitter compounds. In this work, the amphiphilic *p*-sulfonatocalix[4]arenes are used as not only surface-coating agents of QDs, but also as host molecules towards ACh which act at the water–QD interface. We believe that the surface architectures of QDs on introducing the calixarene-based host–guest recognition will afford a variety of molecular sensing systems for chemical and bioanalytical applications.[20]

Notes and references

1 (*a*) C. J. Murphy, *Anal. Chem.*, 2002, **74**, 520A; (*b*) J. Riegler and T. Nann, *Anal. Bioanal. Chem.*, 2004, **379**, 913; (*c*) A. M. Smith and S. Nie, *Analyst*, 2004, **129**, 672; (*d*) P. Alivisatos, *Nat. Biotechnol.*, 2004, **22**, 47.

2 (*a*) A. P. Alivisatos, *J. Phys. Chem.*, 1996, **100**, 13226; (*b*) X. Zhong, Y. Feng, W. Knoll and M. Han, *J. Am. Chem. Soc.*, 2003, **125**, 13559; (*c*) C. B. Murray, S. Sun, W. Gascher, H. Doyle, T. A. Betley and C. R. Kagan, *IBM J. Res. Dev.*, 2001, **45**, 47.

3 A. Watson, X. Wu and M. Bruchez, *BioTechniques*, 2003, **34**, 296.

4 (*a*) M. Bruchez, Jr., M. Moronne, P. Gin, S. Weiss and A. P. Alivisatos, *Science*, 1998, **281**, 2013; (*b*) W. C. W. Chan and S. Nie, *Science*, 1998, **281**, 2016.

5 J. V. Frangioni, *Curr. Opin. Chem. Biol.*, 2003, **7**, 626.

6 (*a*) D. E. Moore and K. Patel, *Langmuir*, 2001, **17**, 2541; (*b*) Y. Chen and Z. Rosenzweig, *Anal. Chem.*, 2002, **74**, 5132; (*c*) K. M. Gattás-Asfura and R. M. Leblanc, *Chem. Commun.*, 2003, 2684; (*d*) J.-G. Liang, X.-P. Ai, Z.-K. He and D.-W. Peng, *Analyst*, 2004, **129**, 619; (*e*) H.-Y. Xie, J.-G. Liang, Z.-L. Zhang, Y. Li, Z.-K. He and D.-W. Peng, *Spectrochim. Acta, Part A*, 2004, **60**, 2527.

7 W. J. Jin, M. T. Fernández-Arguelles, J. M. Costa-Fernández, R. Pereiro and A. Sanz-Medel, *Chem. Commun.*, 2005, 883.

8 L. Qu and X. Peng, *J. Am. Chem. Soc.*, 2002, **124**, 2049.

9 (*a*) M. A. Hines and P. Guyot-Sionnest, *J. Phys. Chem.*, 1996, **100**, 468; (*b*) B. O. Dabbousi, J. Rodriguez-Viejo, F. V. Mikulec, J. R. Heine, H. Mattoussi, R. Ober, K. F. Jensen and M. G. Bawendi, *J. Phys. Chem. B*, 1997, **101**, 9463.

10 (*a*) J.-M. Lehn, R. Meric, J.-P. Vigneron, M. Cesario, J. Guilhem, C. Pascard, Z. Asfari and J. Vicens, *Supramol. Chem.*, 1995, **5**, 97; (*b*) K. N. Koh, K. Araki, A. Ikeda, H. Otsuka and S. Shinkai, *J. Am. Chem. Soc.*, 1996, **118**, 755; (*c*) T. Jin, *J. Inclusion Phenom.*, 2003, **45**, 195.

11 S. Shinkai, S. Mori, H. Koreishi, T. Tsubaki and O. Manabe, *J. Am. Chem. Soc.*, 1986, **108**, 2409.

12 R. Rigler and E. S. Elson, *Fluorescence Correlation Spectroscopy*, Springer-Verlag, Berlin Heidelberg, 2001.

13 $G(\tau)$ is defined as $G(\tau) = < \delta I(\tau)\delta I(0)>/<I(\tau)>^2$, where $I(\tau)$ is the fluorescence intensity at the time τ, and $\delta I(\tau) = I(\tau) - <I(\tau)>$. The brackets denote the ensemble average.

14 (*a*) S. Björling, M. Kinjo, Z. Földes-Papp, E. Hagman, P. Thyberg and R. Rigler, *Biochemistry*, 1998, **37**, 12971; (*b*) M. Kinjo, G. Nishimura, T. Koyama, Ü. Mets and R. Rigler, *Anal. Biochem.*, 1998, **260**, 166; (*c*) N. Yoshida, M. Kinjo and M. Tamura, *Biochem. Biophys. Res. Commun.*, 2001, **280**, 312.

15 Assuming a spherical body of fluorophores, the size of the fluorophores can be evaluated by the following relationship: $r_1/r_2 = \tau_1/\tau_2$, where r_i and τ_i mean the radius and diffusion time of the fluorophore *i*.

16 For estimation of the molecular length of MAA, the CPK (Corey–Pauling–Koltun) molecular model is used.

17 The molecular lengths of TOPO and **3** along with the alkyl chains are estimated as 1.3 nm and 1.6 nm, respectively.

18 T. Jin, F. Fujii, H. Sakata, M. Tamura and M. Kinjo, *Chem. Commun.*, 2005, 2829.

19 J. R. Lakowicz, *Principles of Fluorescence Spectroscopy*, Kluwer Academic/Plenum Publishers, New York, 1999, ch. 8, pp. 238–264.

20 Recently, β-cycodextrin-modified CdS QDs for the control of complexation-induced fluorescence change were reported: K. Palaniappan, S. A. Hackney and J. Liu, *Chem. Commun.*, 2004, 2704.

Analysis of Cellular Functions by Multipoint Fluorescence Correlation Spectroscopy

Y. Takahashi[1,2], R. Sawada[2], K. Ishibashi[2], S. Mikuni[1] and M. Kinjo[1,*]

[1]*Laboratory of Supramolecular Biophysics, Research Institute for Electronic Science, Hokkaido University, Sapporo 060-0812, Japan and* [2]*Olympus Corporation, Tokyo 192-8512, Japan*

Abstract: The biophysical investigation of living cells is currently possible by single molecular detection methods such as fluorescence correlation spectroscopy (FCS). FCS is applied for measuring the dynamic mobility of target molecules in living cells; however, the conventional FCS systems still lack quantitative analysis for many regions of interests (ROI) in real time. To improve this situation, we have developed a novel multipoint FCS system (M-FCS) that can measure multipoint correlation functions in the cell simultaneously. To evaluate its performance, we measured correlation functions for rhodamine 6G (Rh6G) in homogeneous conditions and for green fluorescence protein (GFP) in HeLa cells. We conclude that M-FCS possesses reliable performance. As a pharmacological application, glucocorticoid receptor protein fused GFP (GR-GFP) was transfected in HeLa cells and FCS measurements were carried out in the cytoplasm and the nucleus simultaneously. The translocation of GR-GFP from the cytoplasm to the nucleus by ligand stimulation was observed with laser scanning microscopy (LSM) and M-FCS. Particularly in the nucleus, the slower diffusion of GR-GFP suggested molecular interactions after the translocation. These data imply that M-FCS can be applied for quantitative analysis of kinetic processes in living cells.

Key Words: FCS, multipoint, glucocorticoid receptor, GFP, living cell.

INTRODUCTION

Recent advanced single-molecule-detection technologies for studying molecular behavior in the living cell have been developed with improved optical hardware and also with green fluorescence protein (GFP) and its variants [1]. In observing mobility of molecules, fluorescence recovery (or redistribution) after photobleaching (FRAP) is one of the important imaging techniques for understanding the biophysical status of molecules in the living cell [2-4]. However, FRAP is not a fully sufficient method for this purpose because it can only measure rather slow mobile populations of proteins. Current reports suggest the limitations of the FRAP method and researchers are trying to combine it with other detection methods for highly mobile individual molecules with lower invasive conditions in the living cell [5-7].

For this purpose, fluorescence correlation spectroscopy (FCS) has been developed to detect rapid diffusion of molecules in aqueous solution [8, 9]. Recent studies have demonstrated that FCS is a promising method to study signal transduction in the living cell. For example, the transport mechanisms of protein kinase C (PKC) through the plasma membrane [10], and the signaling pathway of the signal transducer and activator of transcription 3 (STAT3) can be analyzed by FCS [11].

A commercial FCS system in conjunction with laser scanning microscopy (LSM) has been developed by Carl Zeiss (Jena, Germany) for measuring fluorescence-labeled molecules in living cells [12]. This has made it possible to detect the localization of target molecules in live cells by the LSM unit and also their physiological states such as number, size, and mobility of molecules can be analyzed by the FCS unit.

However, with this conventional system it is not possible to observe spatial molecular dynamics occurring at the same time in the cell, because of the limitations of optical hardware. To measure FCS at other points, for example, the sample on the microscope stage has to be moved sequentially to adjust the measurement point to the center of the optical axis. This time lag might be a critical limit for observing the rapid movement of targets in live-cell conditions.

To solve this problem, we present a quantitative experimental approach for multipoint FCS measurement simultaneously. We have developed a multipoint FCS setup (M-FCS) with modified optical hardware and improved analysis software. The maximum number of measurement points is at present four positions, and these can be selected at any place in the area of the acquired LSM image. M-FCS can be used for detecting spatial information at one time; therefore it elucidates kinetic processes occurring in the cell. In this study, we applied M-FCS to determine the diffusion times of fluorescence dye molecules in solution and green fluorescence protein (GFP) in cultured cells.

As a pharmacological application, we used GFP-conjugated GR (GR-GFP) for observing its trafficking from the cytoplasm to the nucleus by ligand stimulation. GR is well known as a transcription factors regulated by glucocorticoid in physiological processes [13]. GR forms a dimer in cytoplasm and this is translocated to nuclei to regulate target

*Address correspondence to this author at the Laboratory of Supramolecular Biophysics, Research Institute for Electronic Science, Hokkaido University, Sapporo 060-0812, Japan; E-mail: kinjo@imd.es.hokudai.ac.jp

This work was presented as a lecture on 'The 7th International Carl Zeiss sponsored Workshop on FCS and Related Methods, October 5-6, 2004, Dresden, Germany'.

1389-2010/05 $50.00+.00

genes, and it also binds with other transcription factors or regulatory proteins to modify their functions [14]. There are many experimental designs for observing these complicated dynamics; however, only a few researchers have reported quantitative analysis of GR dynamics in the living cell. In a previous experiment using FCS, the dimerization of GR-GFP in cytoplasm of Cos7 cells was suggested by the increase of counts per molecule (CPM) [15]. Here, using our M-FCS, we demonstrate simultaneous FCS measurement both in the cytoplasm and in the nucleus, and quantitative evaluation in terms of molecular mobility is discussed.

MATERIALS AND METHODS

Reagents, Cells, and Plasmid DNA Transfection

A low concentration (10^{-7} M) of rhodamine 6G (Rh6G) was prepared in water for the FCS measurement in homogeneous conditions. HeLa cells that stably expressed GFP (GFP-HeLa) were grown in a 5% CO_2 humidified atmosphere at 37 °C in Dulbecco's modified Eagle's medium (DMEM) supplemented with 10% fetal calf serum. Cells were plated on LAB-TEK chambered coverslips (Nalge Nunc International, Naperville, IL, USA), and DMEM was changed to phenol-red-free medium (OPTI-MEM: Gibco, Japan) before FCS measurement. For demonstration of the pharmacological aspect of transcription factors in living cells, HeLa cells were generated by transfection of the expression vectors for glucocorticoid receptor fused with EGFP (GR-GFP) by FuGENE6 (Roche Molecular Biochemicals, Mannheim, Germany). To observe the trafficking of GR-GFP, 1 μM dexamethasone (Dex) was added to GR-GFP-expressing HeLa cells as a ligand-stimulus for GR.

M-FCS Setup and Data Processing

The system consists of two modules including LSM and FCS. The laser unit has five wavelength lines (458, 488, 514, 543, and 633nm). The concept of multipoint FCS measurement is shown in Fig. **1**. The laser beam is focused on each selected point (a, b, and c in Fig. **1A**) sequentially every one second by the movement of a scanner mirror. Fluorescence is collected through a confocal aperture, and directed to photomultiplier tubes (PMT) for image scanning and to an avalanche photodiode (APD) for FCS measurement. To measure FCS, all emitted light is directed to a dichroic mirror, and the emitted light is sent either to one APD for single color autocorrelation function or to two APDs for dual color cross correlation function. In this work, we only measured the single color autocorrelation function with a bandpass filter (510-610nm) for Rh6G or GFP. As shown in Fig. **1B** & **C**, sequentially obtained multipoint fluorescence light is grouped and aligned at each point, and the calculation of the correlation function performed by the software correlators during the measurement. After measurement, the autocorrelation function is fitted to the model as follows,

$$G(\tau) = 1 + \frac{1}{N} \sum \frac{f_i}{\left(1 + \frac{\tau}{\tau_i}\right)\left(1 + \frac{\tau}{\tau_i}\left(\frac{W_{xy}}{W_z}\right)^2\right)^{\frac{1}{2}}} \quad with \sum_i f_i = 1$$

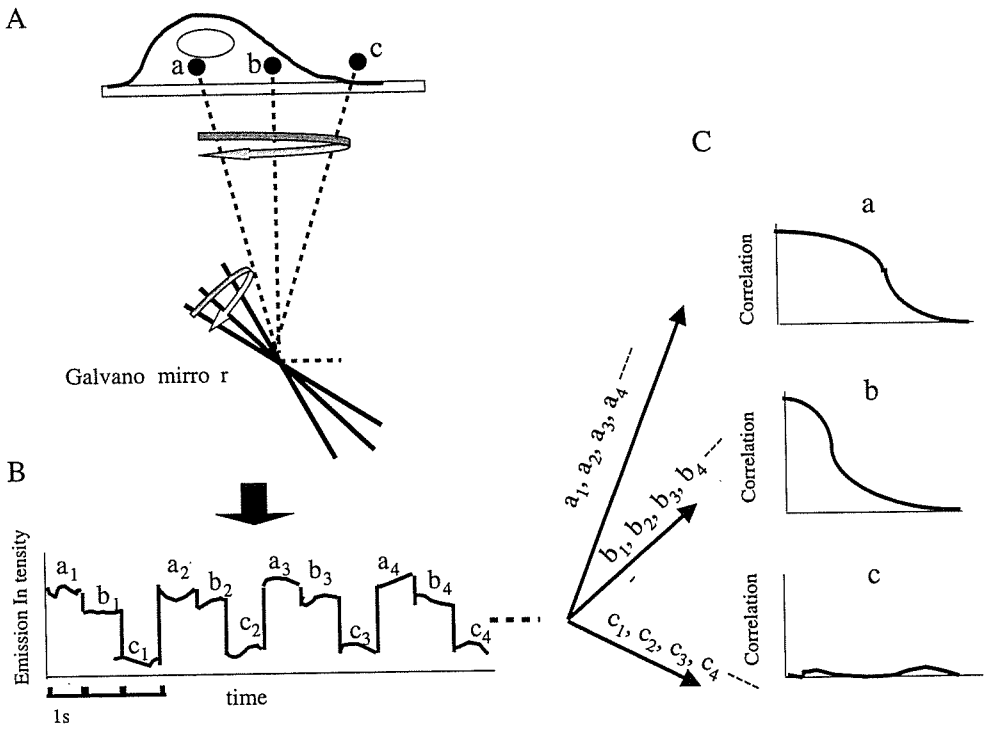

Fig. (1). The basic concept of multipoint FCS measurement. A: The excitation laser beam is focused on three points sequentially (a, b, c, a, b, c, ...) by controlling the scanning of a Galvano mirror. B: Emitted photons are collected and lined up sequentially (a1, b1, c1, a2, b2, c2, ...). C: The data of photon counts are grouped and aligned at each measurement point (a1, a2, a3, a4 ..., b1, b2, b3, b4 ..., c1, c2, c3, c4, etc.), and therefore each correlation function can be obtained.

where N denotes the number of fluorescence molecules, τ_i denotes the diffusion time of the fraction f_i (i=1, 2, 3), and w_{xy}/w_z denotes the axial ratio of the volume element.

This fitting analysis was performed by the Levenberg Marrquard algorithm of Origin Pro 7.5J (OriginLab Corporation, Northampton, MA, USA).

RESULTS AND DISCUSSION

To evaluate the performance of M-FCS, we first measured Rh6G molecules in homogeneous aqueous conditions. Fig. **2** shows the results of simultaneous FCS measurement at four points in the solution. The four selected points were located at the corners of a 40μm square. In these homogeneous conditions, the diffusion constant of Rh6G was expected to be identical everywhere. As shown in Fig. **2B**, all four fluorescence autocorrelation functions (FAFs) were similar and all analyzed values such as diffusion time, count rates, numbers of molecules, and counts per molecule (Fig. **2C**) showed low deviation (less than 5%) among the four measurement points. This demonstrated the reliable performance of M-FCS and this system was adequate for obtaining accurate results without any problem of mechanical movement of hardware and the calculation of autocorrelation functions. This accuracy of M-FCS measurement indicates that reliable performance can be expected even in a heterogeneous system such as a live cell.

To further assess the precision of M-FCS, we used HeLa cells stably expressing GFP as indicated in Fig. **3**. The LSM image shows four HeLa cells expressing GFP distributed in all areas of the cell. Although all four cells showed similar levels of fluorescence intensity in the LSM image, the mean number of GFP molecules detected in a measurement volume was varied from 33 (cell 4) to 53 (cell 3). The diffusion time of GFP in each cell was almost the same (0.21 – 0.28 msec). This means that stably expressed GFP in HeLa cells moved freely in cell although the concentration of GFP differed.

For more detailed observation, M-FCS measurement was carried out in a single HeLa cell expressing GFP. The LSM image of a single cell at large magnification can indicate the complicated structure of the cell as shown in Fig. **4A**. Two positions (1 and 4) were located in the cytoplasm and the other two positions (2 and 3) were in the nucleus. The location of position 3 was in the nucleolus, which was obviously shown as a dark spot in the LSM image. Fig. **4B** indicates that only one autocorrelation function in the area of the nucleolus (position 3) showed a significantly higher value of G (0). This indicated lower number of GFP molecules in the nucleolus (N=36 at position 3) than in the other three positions and agreed with the lower intensity of the LSM image of the nucleolus. Although the number of GFP molecules in the nucleolus was significantly lower, the diffusion time at the nucleolus was slightly slower (DT=0.29 msec) than those at the other three positions. This slower diffusion of GFP may indicate the complex structure of the nucleolus. As the nucleolus is a nuclear subcompartment and its biological function is one of the key factors for dynamic protein processing [16], M-FCS might be a useful tool for differencing the status of molecular dynamics in each local area in the nucleus.

A

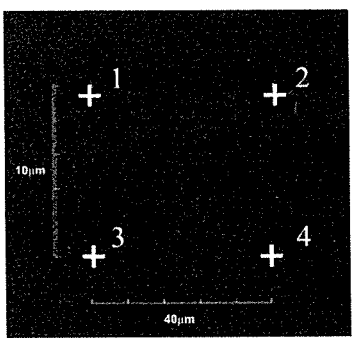

B

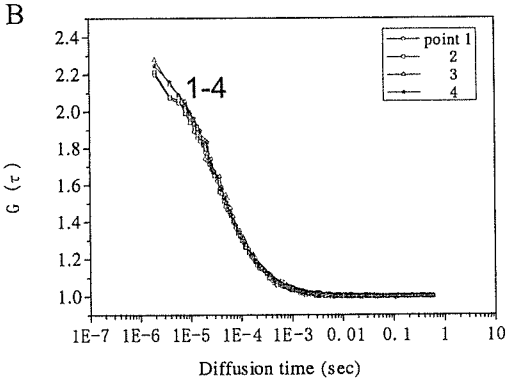

C

point	DT (μ sec)	CR (kHz)	N	CPM (kHz)
1	37.4	19.6	0.82	23.8
2	35.7	19.4	0.81	23.9
3	36.4	20.1	0.78	25.8
4	34.9	20.7	0.78	26.7
Mean ± SD	36.1 ± 0.9	19.9 ± 0.5	0.79 ±0.02	25.1 ±1.2

Fig. (2). Simultaneous M-FCS measurement at four points in homogeneous Rh6G solution.

A: Four selected measurement points are shown in the LSM image. The points are at the corners of a 40 μm square. B: FAFs of Rh6G at the four measurement points. C: Differences of the diffusion times (DT), count rates (CR), numbers of molecules (N), and counts per molecule (CPM) among the four measurement points.

A

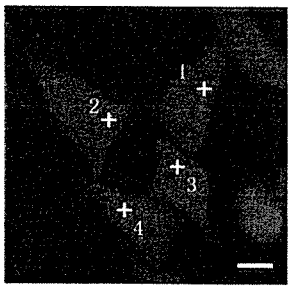

B

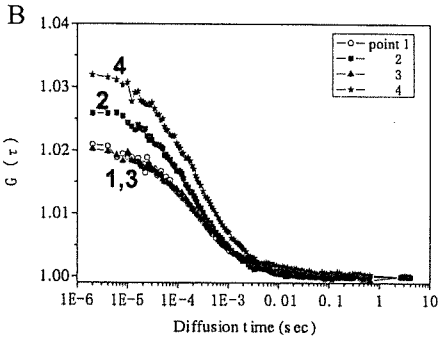

C

point	DT (msec)	CR (kHz)	N	CPM (kHz)
1	0. 26	413	52	7. 9
2	0. 21	532	40	13. 5
3	0. 28	565	53	10. 7
4	0. 27	433	33	12. 9

Fig. (3). M-FCS measurement of four HeLa cells stably expressing GFP.

A: LSM image of cells and four marked measurement points (1, 2, 3 and 4). Scale bar represents 10 μm. B: FAFs of GFP in four independent cells. Numbers marked on FAFs correspond with the numbers on the LSM image (A). C: Differences of the diffusion times (DT), count rates (CR), numbers of molecules (N), and counts per molecule (CPM) among the four cells.

A

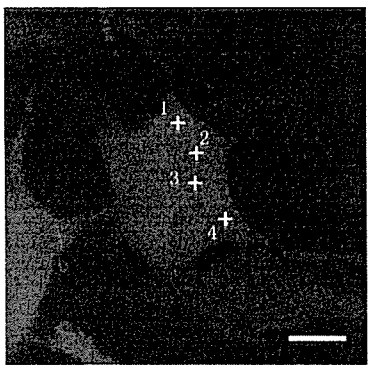

B

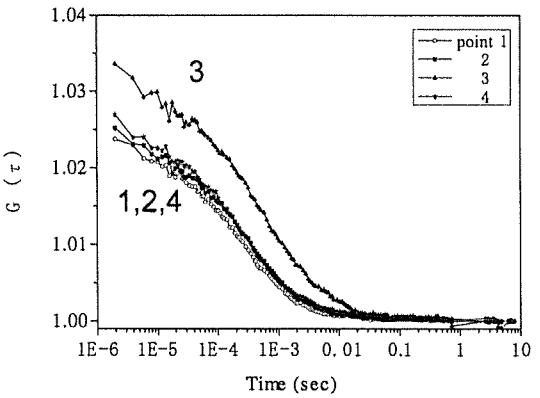

C

point	DT (msec)	CR (kHz)	N	CPM (kHz)
1	0. 27	474	51	9. 4
2	0. 25	432	48	9. 1
3	0. 29	251	36	7. 0
4	0. 25	468	45	10. 5

Fig. (4). M-FCS measurement in a single HeLa cell stably expressing GFP.

A: LSM image of a single cell and four FCS measurement points. Scale bar represents 10 μm. B: The four FAFs obtained from four measurement points correspond with the numbers marked in the LSM image (A). C: Differences of the diffusion times (DT), count rates (CR), numbers of molecules (N), and counts per molecule (CPM) among four points in a single cell.

To evaluate the performance of M-FCS, we employed this system for a pharmacological application. The dynamic movement of GR molecules from the cytoplasm to the nucleus was observed after stimulation with dexamethasone (Dex). The time courses of LSM images are shown in Fig. **5A** (a-f). The fluorescence intensity of GR-GFP in the cytoplasm was much higher than that in the nucleus at the pre-stimulation time (a), and this contrast gradually changed after stimulation (b-f). Finally, at 13min after the stimulation, the fluorescence intensity of GFP in the nucleus increased and therefore, the image of GR in the cytoplasm faded away. The speed of GR transport from the cytoplasm to the nucleus